Title

Asymmetric Expression of LincGET Biases Cell Fate in Two-Cell Mouse Embryos

Journal

Cell, 175(7)

ISSN

0092-8674

Authors

Wang, Jiaqiang
Wang, Leyun
Feng, Guihai
et al.

Publication Date

2018-12-01

DOI

10.1016/j.cell.2018.11.039

Peer reviewed

Article

Cell

Asymmetric Expression of *LincGET* Biases Cell Fate in Two-Cell Mouse Embryos

Graphical Abstract

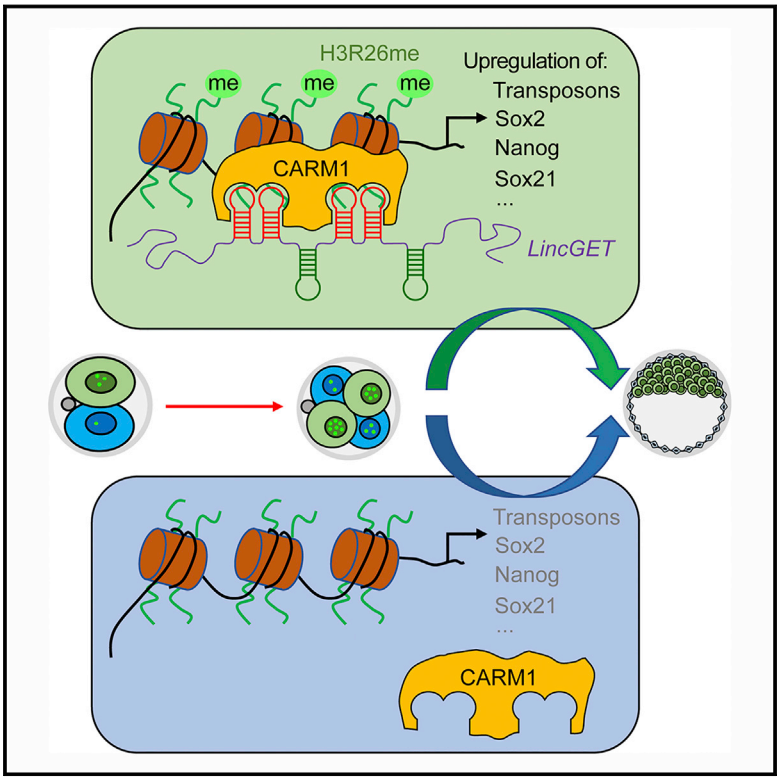

Authors

Jiaqiang Wang, Leyun Wang, Guihai Feng, ..., Zhonghua Liu, Wei Li, Qi Zhou

Correspondence

liwei@ioz.ac.cn (W.L.), qzhou@ioz.ac.cn (Q.Z.)

In Brief

An endogenous retrovirus-associated nuclear long noncoding RNA biases cell fate in mouse two-cell embryos.

Highlights

- *LincGET* is asymmetrically expressed in the nucleus of two- to four-cell mouse embryos
- *LincGET* overexpression biases blastomere fate toward inner cell mass (ICM)
- *LincGET* physically binds to CARM1
- *LincGET*/CARM1 activates ICM-specific genes

Data Resources

GSE110419

Wang et al., 2018, Cell *175*, 1887–1901
December 13, 2018
https://doi.org/10.1016/j.cell.2018.11.039

CellPress

Article

Cell

Asymmetric Expression of *LincGET* Biases Cell Fate in Two-Cell Mouse Embryos

Jiaqiang Wang,[1,2,3,4,8] Leyun Wang,[1,8] Guihai Feng,[1,8] Yukai Wang,[1,8] Yufei Li,[1,2] Xin Li,[5,6] Chao Liu,[1,2] Guanyi Jiao,[1,2] Cheng Huang,[1,2] Junchao Shi,[7] Tong Zhou,[7] Qi Chen,[7] Zhonghua Liu,[4] Wei Li,[1,2,3,*] and Qi Zhou[1,2,3,9,*]

[1]State Key Laboratory of Stem Cell and Reproductive Biology, Institute of Zoology, Chinese Academy of Sciences, 100101 Beijing, China
[2]University of Chinese Academy of Sciences, 100049 Beijing, China
[3]Institute for Stem Cell and Regeneration, Chinese Academy of Sciences, 100101 Beijing, China
[4]College of Life Science, Northeast Agricultural University, 150030 Harbin, China
[5]Institute for Genomic Medicine, University of California, San Diego, CA 92093, USA
[6]Department of Ophthalmology, University of California, San Diego, CA 92093, USA
[7]Department of Physiology and Cell Biology, University of Nevada, Reno School of Medicine, Reno, NV 89557, USA
[8]These authors contributed equally
[9]Lead Contact
*Correspondence: liwei@ioz.ac.cn (W.L.), qzhou@ioz.ac.cn (Q.Z.)
https://doi.org/10.1016/j.cell.2018.11.039

SUMMARY

In early mammalian embryos, it remains unclear how the first cell fate bias is initially triggered and amplified toward cell fate segregation. Here, we report that a long noncoding RNA, *LincGET*, is transiently and asymmetrically expressed in the nucleus of two- to four-cell mouse embryos. Overexpression of *LincGET* in one of the two-cell blastomeres biases its progeny predominantly toward the inner cell mass (ICM) fate. Mechanistically, *LincGET* physically binds to CARM1 and promotes the nuclear localization of CARM1, which can further increase the level of H3 methylation at Arginine 26 (H3R26me), activate ICM-specific gene expression, upregulate transposons, and increase global chromatin accessibility. Simultaneous overexpression of *LincGET* and depletion of *Carm1* no longer biased embryonic fate, indicating that the effect of *LincGET* in directing ICM lineage depends on CARM1. Thus, our data identify *LincGET* as one of the earliest known lineage regulators to bias cell fate in mammalian 2-cell embryos.

INTRODUCTION

Long noncoding RNAs (lncRNAs) have recently emerged as key regulators of many important biological events (Rinn and Chang, 2012), including controlling stem cell pluripotency and differentiation (Guttman et al., 2011; Hu et al., 2012; Ng and Stanton, 2013). However, it remains unknown whether lncRNAs are also actively involved in the process of early embryonic cell fate decision, such as the first lineage segregation that bifurcate the totipotent zygote into the inner cell mass (ICM), which contributes to the fetus, and the trophectoderm (TE), which contributes to the placenta.

In mammalian early embryonic development, the blastomeres within an embryo are morphologically indistinguishable before the eight-cell stage, and their fates are relatively flexible depending on the regulative nature of mammalian embryo development (Rossant and Tam, 2009). However, recent emerging studies have provided compelling evidence that molecular heterogeneity already exists in four- to eight-cell-stage embryos, which predispose the fate of early blastomeres toward either ICM or TE (Goolam et al., 2016; Piotrowska-Nitsche et al., 2005; Plachta et al., 2011; Tabansky et al., 2013; Torres-Padilla et al., 2007; White et al., 2016). To date, the earliest molecular heterogeneity documented was at the four-cell embryo stage. Coactivator-associated arginine methyltransferase 1 (CARM1) was first found asymmetrically distributed between four-cell blastomeres in mice; high CARM1 led to increased levels of histone H3 arginine 26 methylation (H3R26me), which biased the subsequent fate of these blastomeres toward ICM (Torres-Padilla et al., 2007). Recent evidence further showed that high expression of CARM1 at the four-cell stage also increased the OCT4/SOX2-DNA-bound fraction and the expression of its downstream target gene, such as *Sox21* (Goolam et al., 2016; Plachta et al., 2011; White et al., 2016). In addition, PRDM14 was found to be heterogeneously expressed in four-cell-stage embryos, and it interacted with CARM1 to promote H3R26me (Burton et al., 2013). Together, elevation of proteins in the CARM1/PRDM14-OCT4/SOX2-SOX21 axis at the four-cell stage will bias the future progeny of blastomeres toward an ICM fate.

Despite these advances, a key question still remains as to how the observed heterogeneity at the four-cell stage arises in the first place. Is the factor responsible for such heterogeneity buried at the two-cell stage and controlled by upstream regulators? Indeed, with recent research advances using single-blastomere RNA sequencing (RNA-seq), we found that blastomere-to-blastomere heterogeneity already exists at the two-cell stage (Shi et al., 2015). Moreover, we recently found that an endogenous retrovirus (ERV)-associated lncRNA, *LincGET*, was expressed along with zygotic genome activation (ZGA) and specifically persisted through the late two- to four-cell mouse embryo stage, and that *LincGET* was essential for

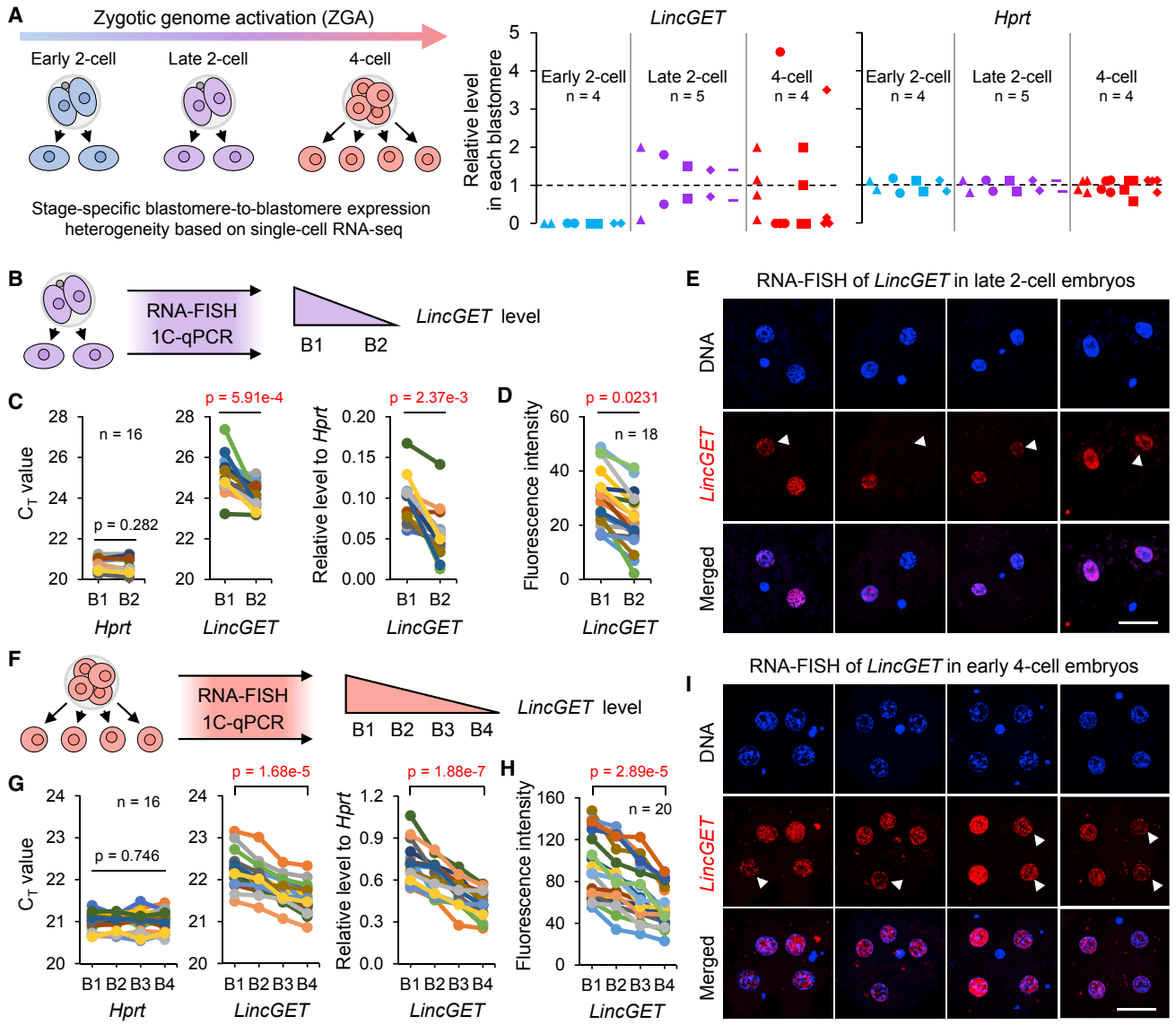

Figure 1. *LincGET* is Transiently Expressed and Asymmetrically Distributed in Two- to Four-Cell Blastomeres

(A) *LincGET* expression is heterogeneous (compared with *Hprt*) in two- to four-cell embryos, according to the bioinformatic analyses of single-blastomere RNA-seq data. Hprt work as a control that is symmetry distributed among blastomeres in two- to four-cell embryos.

(B and F) Schematic overview. Late two-cell (B) or early four-cell (F) embryos were harvested for RNA-FISH and digested into single blastomeres for single-cell (1C)-qPCR. Blastomeres are named B1 and B2 (B) or B1 to B4 (F) according to decreasing *LincGET* concentration.

(C and G) 1C-qPCR results showing *LincGET* distribution asymmetry between blastomeres of late two-cell embryos (C) or among blastomeres of early four-cell embryos (G), but not the housekeeping gene, *Hprt*. CT values are used for level analysis. Two-tailed Student's t tests were used for the statistical analysis.

(D and H) Quantification of RNA-FISH fluorescence intensity of embryos in (B) and (F) showing the asymmetric distribution of *LincGET* at the late two-cell (D) or early four-cell (H) stage. Intensity relative to DNA signal was used.

(E and I) Examples of RNA-FISH of late two-cell (E) or early four-cell (I) embryos. Nuclei with lower *LincGET* are marked by white arrow heads. Three experimental replicates were performed. Scale bar, 50 μm.

See also Figure S1.

embryo development (Wang et al., 2016). Intriguingly, when we analyzed blastomere-to-blastomere heterogeneity of *LincGET* expression using single-blastomere RNA-seq datasets (Deng et al., 2014), we found that its level of expression from the late two-cell blastomere stage became unequal, and this asymmetric distribution was further enhanced in four-cell blastomeres (Figure 1A). These observations led to the present systematic analyses of the heterogeneity of *LincGET* in mouse early embryos and its role in regulating CARM1 level and function to bias the first fate of the embryonic cell.

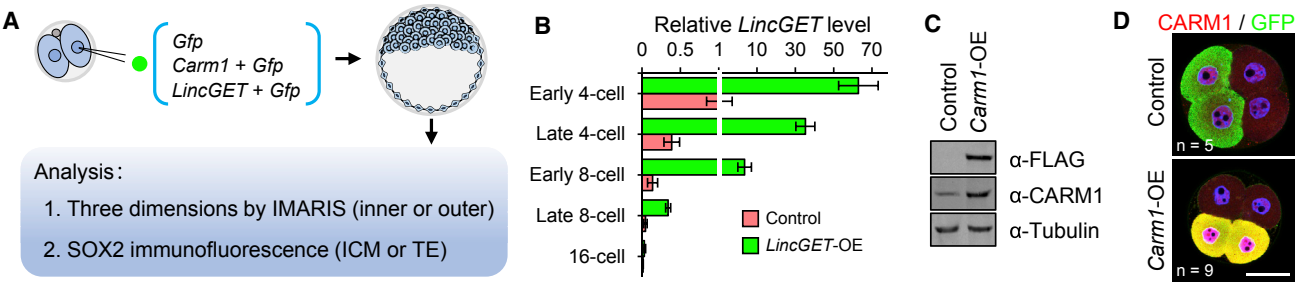

E

Group	Blastocysts 3D (%)	Total cells (n)	Inner cells (%)	GFP cells (%)	Inner cells that are GFP$^+$ (%)	GFP cells that are inner (%)
Gfp	65 (82.65)	41.91 ± 8.79	(37.68 ± 3.43)	(49.02 ± 3.44)	(53.06 ± 8.03) ^{x}	(40.51 ± 4.60) ^{x}
Carm1 + Gfp	63 (84.47)	43.65 ± 10.09	(37.05 ± 2.87)	(48.16 ± 3.02)	(82.45 ± 11.10) ^{y}	(63.38 ± 8.55) ^{y}
LincGET + Gfp	64 (85.18)	47.58 ± 10.35	(37.27 ± 2.52)	(48.40 ± 2.79)	(85.15 ± 9.17) ^{y}	(65.52 ± 7.26) ^{y}

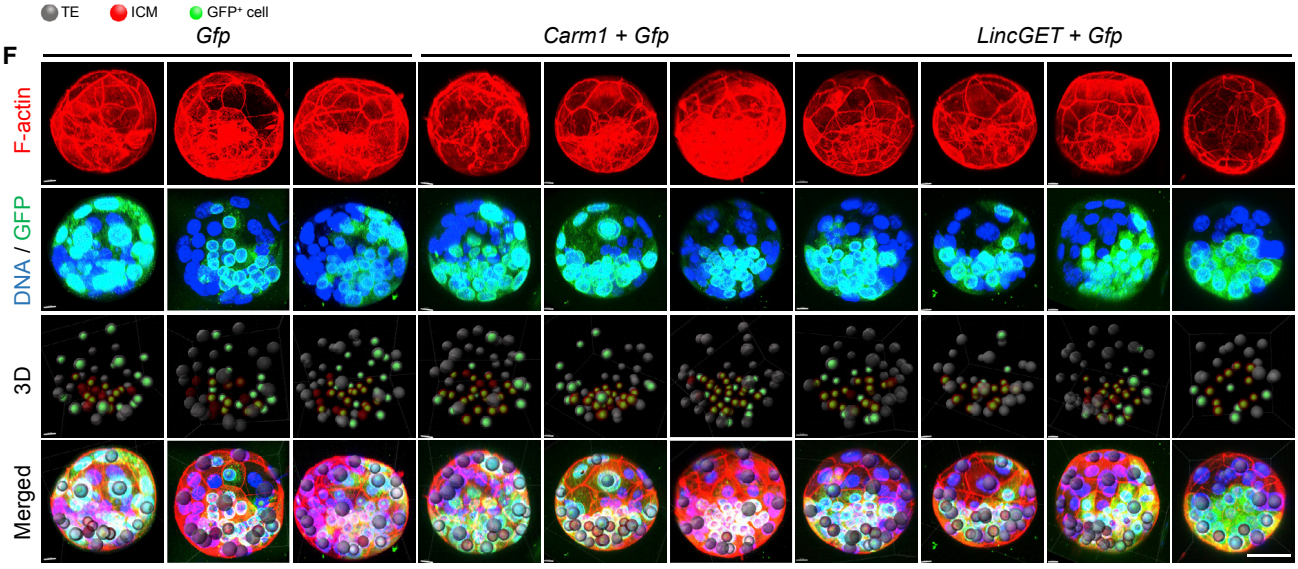

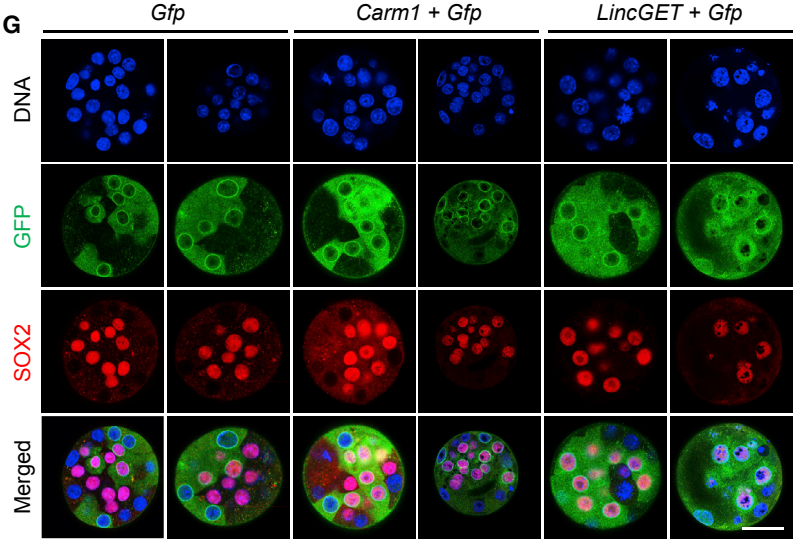

H

Group	Cross sections	GFP cells that are SOX2$^+$ (%)
Gfp	7	(43.57 ± 11.39) ^{x}
Carm1 + Gfp	7	(74.63 ± 15.05) ^{y}
LincGET + Gfp	7	(84.22 ± 14.45) ^{y}

(legend on next page)

RESULTS

LincGET is Transiently Expressed and Asymmetrically Distributed in Two- to Four-Cell Blastomeres

To systematically examine the spatiotemporal expression of *LincGET* in early mouse embryos, we performed fluorescence *in situ* hybridization (FISH) and quantitative PCR with TaqMan probe (TM-qPCR), targeting the *LincGET*-specific region (2,591–2,780 nt) (Figure S1A) throughout mouse early preimplantation embryo development. The TM-qPCR results reinforced our bioinformatics analysis, showing transient *LincGET* expression at the two- to four-cell stage (Figures S1B and S1C). Moreover, the FISH (Figure S1D) and northern blotting (Figure S1E) analyses further confirmed that *LincGET* expression is restricted to the nuclei, appearing first at the early two-cell stage followed by upregulation through the late two-cell to early four-cell stage, downregulation through the late four-cell to early eight-cell stage, and subsequently lack of detection at the late eight-cell stage.

Notably, we observed heterogeneous *LincGET* expression in two- to four-cell embryos based on fluorescence intensity and single-blastomere TM-qPCR (1C-qPCR) analyses, which was consistent with our bioinformatics analyses (Figure 1A). Blastomere-to-blastomere expression of *LincGET* was highly variable between two-cell (Figures 1B–1E) and four-cell blastomeres (Figures 1F–1I) compared to the overall equal expression of *Hprt* between blastomeres (Figures 1C and 1G). Moreover, it is notable that the extent of heterogeneous expression of *LincGET* in four-cell blastomeres was further increased compared to that in two-cell embryos (Figures 1C and 1G). Together, these data raised the possibility that *LincGET* may play a role in directing the developmental fates of early blastomeres.

Increased *LincGET* Biased Blastomeres toward an ICM Fate

To test whether *LincGET* plays a role in biasing early blastomere fate, we overexpressed *LincGET* by injecting *LincGET* RNA into one of the two-cell blastomeres, with a co-injection of green fluorescent protein-Klarsicht/ANC-1/Syne-1 homology (GFP-KASH; *Gfp*) RNA as a lineage tracer, and then monitored embryo development to the blastocyst stage (Figure 2A). We documented an elevated level of *LincGET* by TM-qPCR at the four- to eight-cell stages after two-cell stage overexpression, yet the elevation quickly decreased by the late eight-cell stage and decreased almost down to normal levels at the 16-cell stage (Figure 2B). These findings suggested that the turnover of injected *LincGET* RNA was regulated similarly to the endogenously expressed *LincGET*.

To examine the function of *LincGET* in biasing early embryonic fate, we also performed a parallel *Carm1*-overexpression analysis as a positive control. This was achieved by similarly injecting *Carm1* mRNA and the *Gfp* tracer into one of the two-cell blastomeres followed by expression validation at the four-cell stage (Figures 2C and 2D), as previous research has demonstrated that overexpression of *Carm1* in one of the two-cell blastomeres can bias embryo lineage fate (Torres-Padilla et al., 2007). Injection of only the *Gfp* tracer into one of the two-cell blastomeres served as a negative control. The embryos overexpressing either *LincGET* or *Carm1* (about 150 ng/μL) developed normally and reached the blastocyst stage and birth similar to those injected with only the *Gfp* tracer (Figure 2E and Table S1), showing that overexpression of *LincGET* or *Carm1* does not adversely affect embryo development.

We next analyzed the GFP-positive cell population in the resulting blastocysts from the three experimental groups (*Gfp* only, *LincGET + Gfp*, and *Carm1 + Gfp*). The blastocysts used for cell allocation analysis were processed for cortical F-actin staining to show membrane boundaries (Torres-Padilla et al., 2007) such that the contribution of GFP-labeled cells to the inner (ICM) or outer (TE) layer of the blastocyst could be distinguished and analyzed (Figure 2E). As shown in Figure 2E, the total number of cells in blastocysts and the percentage of GFP-positive cells were similar among different groups. However, the percentage of GFP-positive cells in the ICM was significantly higher in the *LincGET + Gfp* (85.15% ± 9.17%) and *Carm1 + Gfp*

Figure 2. Increased *LincGET* Biased Blastomeres toward an ICM Fate

(A) Schematic overview. RNA (*Gfp*, *Carm1 + Gfp*, or *LincGET + Gfp*) was injected into one blastomere of late two-cell embryos, and the distributions of GFP-positive cells were analyzed at the blastocyst stage (1) in three dimensions to view the inner or outer patterns and (2) by SOX2 immunofluorescence (IF) for the ICM or TE pattern. Nuclear-membrane-localized GFP-KASH (*Gfp*) was used as a lineage tracer.

(B) TM-qPCR results confirming the overexpression of *LincGET*. Three experimental replicates were performed. The error bars represent SEM.

(C and D) Western blot (C) and IF (D) results confirming the overexpression of CARM1. Three experimental replicates were performed. OE, overexpression; α-, anti-. Scale bar, 50 μm.

(E) Analysis of the distribution of progeny of injected blastomere at the blastocyst stage based on 3D reconstruction. Data were represented as mean ± SEM. Two-tailed Student's t tests were used for statistical analysis. Different letters (between x and y) indicate very significant differences ($p < 0.00001$). Key to table headings: blastocyst 3D (%) is the number and developmental rate of blastocysts that were all used for the 3D analysis, total cells (n) is the total number of cells in the blastocyst, inner cells (%) is the percentage of inner cells out of the total number of cells in the blastocyst, GFP cells (%) is the percentage of GFP-positive cells out of the total number of cells in the blastocyst, GFP cells that are inner (%) is the percentage of GFP-positive inner cells out of the total number of GFP-positive cells in the blastocyst, inner cells that are GFP^+ (%) is the percentage of GFP-positive inner cells out of the total number of inner cells in the blastocyst, and GFP cells that are inner (%) is the percentage of GFP-positive inner cells out of the total number of total cells in the blastocyst.

(F) Examples of 3D analysis results. Scale bar, 50 μm.

(G) SOX2 and GFP fluorescent staining of blastocysts. SOX2 was used as an ICM marker. The results show that most SOX2-positive cells are GFP-positive in embryos injected with *Carm1* and *Gfp* (*Carm1 + Gfp* lane) or *LincGET* and *Gfp* (*LincGET + Gfp* lane), but not in embryos injected with only *Gfp* (*Gfp* lane). Three experimental replicates were performed. Scale bar, 50 μm.

(H) Statistical data of the percentages of GFP- and SOX2-positive cells out of the SOX2-positive cells of embryos in (G) and Figure S2C. About 40% of GFP-positive cells were SOX2-positive in the control group, while the percentage was about 80% for the *Carm1 + Gfp* and *LincGET + GFP* groups. Two-tailed Student's t tests were used for statistical analysis. Different letters (between x and y) indicate very significant differences ($p < 0.00001$).

See also Figure S2, and Tables S1, S2, and S3.

A

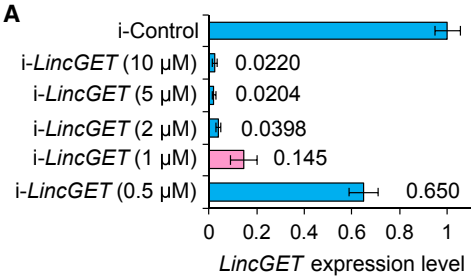

B

Group	Concentration	Injected 2C	4C(%)	BL(%)
i-Control	10 μM	41	39 (90.70)	36 (83.72)
i-*LincGET* 10 μM	10 μM	77	0 (0.00)	0 (0.00)
i-*LincGET* 5 μM	5 μM	84	1 (1.19)	0 (0.00)
i-*LincGET* 2 μM	2 μM	76	1 (1.32)	0 (0.00)
i-*LincGET* 1 μM	1 μM	74	55 (73.33)	33 (44.22)
i-*LincGET* 0.5 μM	0.5 μM	75	70 (94.59)	66 (89.19)

C

Group	Blastocysts 3D (%)	Total cells (n)	Inner cells (%)	GFP cells (%)	Inner cells that are GFP$^+$ (%)	GFP cells that are inner (%)
Gfp	65 (82.65)	41.91 ± 8.79	(37.68 ± 3.43)	(49.02 ± 3.44) ^{x}	(53.06 ± 8.03) ^{x}	(40.51 ± 4.60) ^{x}
i-Control + *Gfp*	36 (83.72)	39.17 ± 6.58	(37.44 ± 3.10)	(49.31 ± 2.84) ^{x}	(54.76 ± 8.00) ^{x}	(41.41 ± 5.47) ^{x}
i-*LincGET* + *Gfp*	33 (44.22)	37.82 ± 6.59	(34.97 ± 2.56)	(40.11 ± 5.17) ^{y}	(31.74 ± 10.49) ^{y}	(27.65 ± 8.41) ^{y}

D

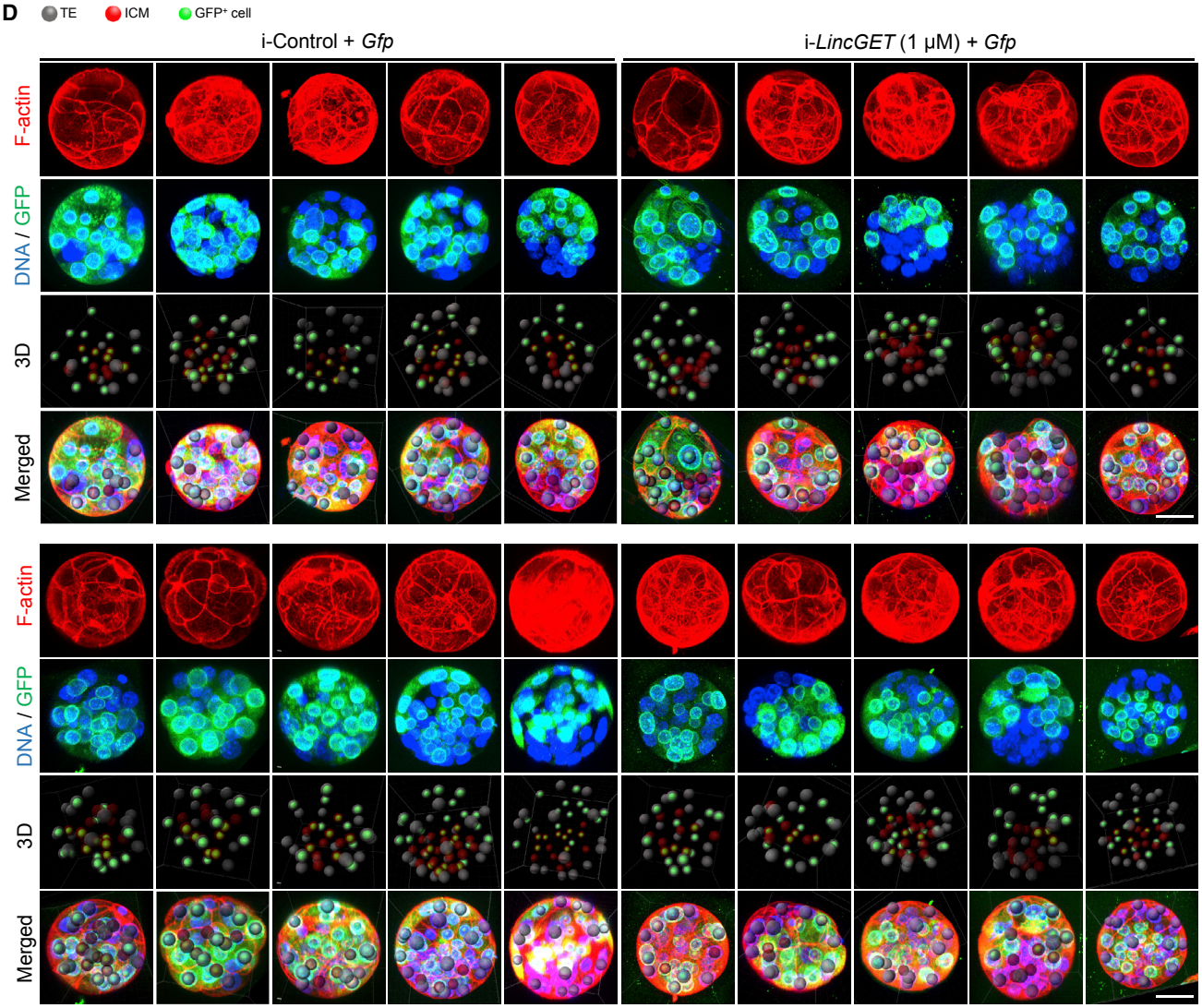

(legend on next page)

(82.45% ± 11.10%) groups than in the *Gfp* only (53.06% ± 8.03%) group (Figures 2E, 2F, S2A, and S2B, and Table S2). Moreover, we examined the expression of SOX2 as an ICM marker in the blastocysts from the three groups and found that the percentage of SOX2-positive cells at the blastocyst stage was much higher in GFP-positive cells derived from both the *LincGET + Gfp* (84.22% ± 14.45%) and *Carm1 + Gfp* (74.63% ± 15.05%) groups than the *Gfp* only (43.57% ± 11.39%) group (Figures 2H and S2C and Table S3). These results demonstrated that forced overexpression of *LincGET* in one of the two-cell blastomeres biased its progeny cells toward an ICM fate.

In order to exclude the possibility that the phenotypic observations may be caused by the large amounts of synthetic RNA being injected, we injected a set of controls: *Dyei*, another mouse ERV-associated lncRNA that has been identified from the genome locus near *LincGET* (between Dyrk1b and Eid2 on chromosome 7) and expressed at the two- to four-cell stages (Wang et al., 2016); *pancIl17d*, a promoter-associated nocoding RNA with interleukin-17d, which is expressed at the two- to four-cell stages and promotes the expression of interleukin-17d from the four-cell stage (Hamazaki et al., 2015); 1–2,570 nt of *LincGET*; 3,940–6,285 nt of *LincGET*; and antisense of ampicillin restriction gene (*antiAmpR*). We found that all of these controls have no effect on preimplantation development, as blastocyst rate and GFP-positive cell rate were normal, and none of the controls could bias fate (Figure S3).

Knockdown of *LincGET* Expression Prevents Blastomeres from Undergoing an ICM Fate

On the other hand, we wondered whether *LincGET* knockdown could prevent blastomeres from undergoing an ICM fate. Our previous study showed that near-complete depletion of *LincGET* in single-cell embryos resulted in a two-cell-stage arrest (Wang et al., 2016), suggesting *LincGET* played an essential role in early embryo development. Thus, to study how *LincGET* knockdown affected cell fate, we performed a knockdown titration assay. The knockdown reagent locked nucleic acid (LNA) was injected into single blastomeres of two-cell embryos at different concentrations followed by analysis of the effect on embryo development. *LincGET* LNA injection into single blastomeres of two-cell embryos at 10 μM, 5 μM, or 2 μM resulted in more than 94% deletion of *LincGET*, and nearly all injected blastomeres exhibited two-cell-stage developmental arrest (Figures 3A and 3B). Besides, *LincGET* LNA injection at 1 μM depleted about 85.5% of total *LincGET*, and 44% of injected blastomeres could still develop to the blastocyst stage while others arrested at the two-cell stage (Figures 3A and 3B). Moreover, injection of *LincGET* LNA at 0.5 μM was unable to knock down *LincGET* efficiently and had little effect on preimplantation development of injected blastomeres (Figures 3A and 3B).

We therefore analyzed the fate choice in the blastocysts after injection of 1 μM *LincGET* LNA into single blastomeres at the two-cell stage. The ratio of progeny with an ICM fate was significantly reduced when the blastomeres were injected with the *LincGET* LNA compared with blastomeres without injection or injected with the control LNA, indicating that a lower level of *LincGET* prevented blastomeres undergoing an ICM fate (Figures 3C and 3D). Furthermore, we found that these blastocysts had a lower percentage of GFP-positive cells (Figures 3C and 3D), indicating that lower levels of *LincGET* do harm preimplantation development.

LincGET and CARM1 Form a Complex

By performing co-localization of *LincGET* via FISH and CARM1 via immunofluorescence staining (IF combined with FISH [IF-coFISH]), we found that in most of the examined early four-cell embryos (eight out of nine), the nuclear intensity of *LincGET* and CARM1 were positively correlated (Figures 4A, 4B, and S4). Moreover, we found that the signals of *LincGET* and CARM1 largely overlapped in the nuclei of early four-cell blastomeres, and more CARM1 located to the nucleus where *LincGET* is higher (Figures 4A and S4). These data raised the possibility that *LincGET* may physically interact with CARM1 to form a functional complex and promote CARM1 nuclear location. We also injected *Dyei* into single-cell embryos (1–2 pL, 150 ng/μL, because its level is very low in four-cell embryos) and performed IF-coFISH at the four-cell stage as a staining control. The results show that *Dyei* does not co-localize with CARM1 (Figure S5).

We separated four-cell embryos into cytoplasmic and nuclear fractions, one blastomere of which was injected with *LincGET* + *Gfp*, *Gfp* only, or *Dyei* + *Gfp* at two-cell stage, and evaluated CARM1 protein level by western blotting. The results showed that *LincGET*, but not *Dyei* or *Gfp* overexpression increased the nuclear percentage of CARM1 (Figure 4C). We

Figure 3. Knockdown of *LincGET* Expression Prevents Blastomeres from Undergoing an ICM Fate

(A) Titration study to knock down *LincGET* using LNA at different concentrations. The TM-qPCR results showed that LNA injection at 10 μM, 5 μM, or 2 μM resulted in more than 94% deletion of *LincGET*; LNA injection at 1 μM and 0.5 μM resulted in depletion of 85.5% and 35% of total *LincGET* level, respectively. Three experimental replicates were performed. The error bars represent SEM.

(B) Preimplantation developmental rate upon *LincGET* knockdown by LNA injection in one blastomere at the two-cell stage. Nearly all the injected blastomeres were arrested at the two-cell stage when injected with *LincGET* LNA at 10 μM, 5 μM, or 2 μM; 44% of blastomeres injected with *LincGET* LNA at 1 μM could develop to blastocyst stage; and *LincGET* LNA injection at 0.5 μM had no effect on preimplantation development of injected blastomeres.

(C) Analysis of the distribution of progeny of injected blastomeres at the blastocyst stage based on 3D reconstruction. LNA for *LincGET* was at 1 μM. Data are shown as mean ± SEM. Two-tailed Student's t tests were used for statistical analysis. Different letters (between x and y) indicate very significant differences ($p < 0.00001$). Key to table headings: blastocyst 3D (%) is the number and developmental rate of blastocysts that were all used for 3D analysis, total cells is the total number of cells in the blastocyst, inner cells (%) is the percentage of inner cells out of the total number of cells in the blastocyst, GFP cells (%) is the percentage of GFP-positive cells out of the total number of cells in the blastocyst, GFP cells that are inner (%) is the percentage of GFP-positive inner cells out of the total number of GFP-positive cells in the blastocyst, and inner cells that are GFP^+ (%) is the percentage of GFP-positive inner cells out of the total number of inner cells in the blastocyst.

(D) Examples of 3D analysis results. Scale bar, 50 μm.

See also Table S2.

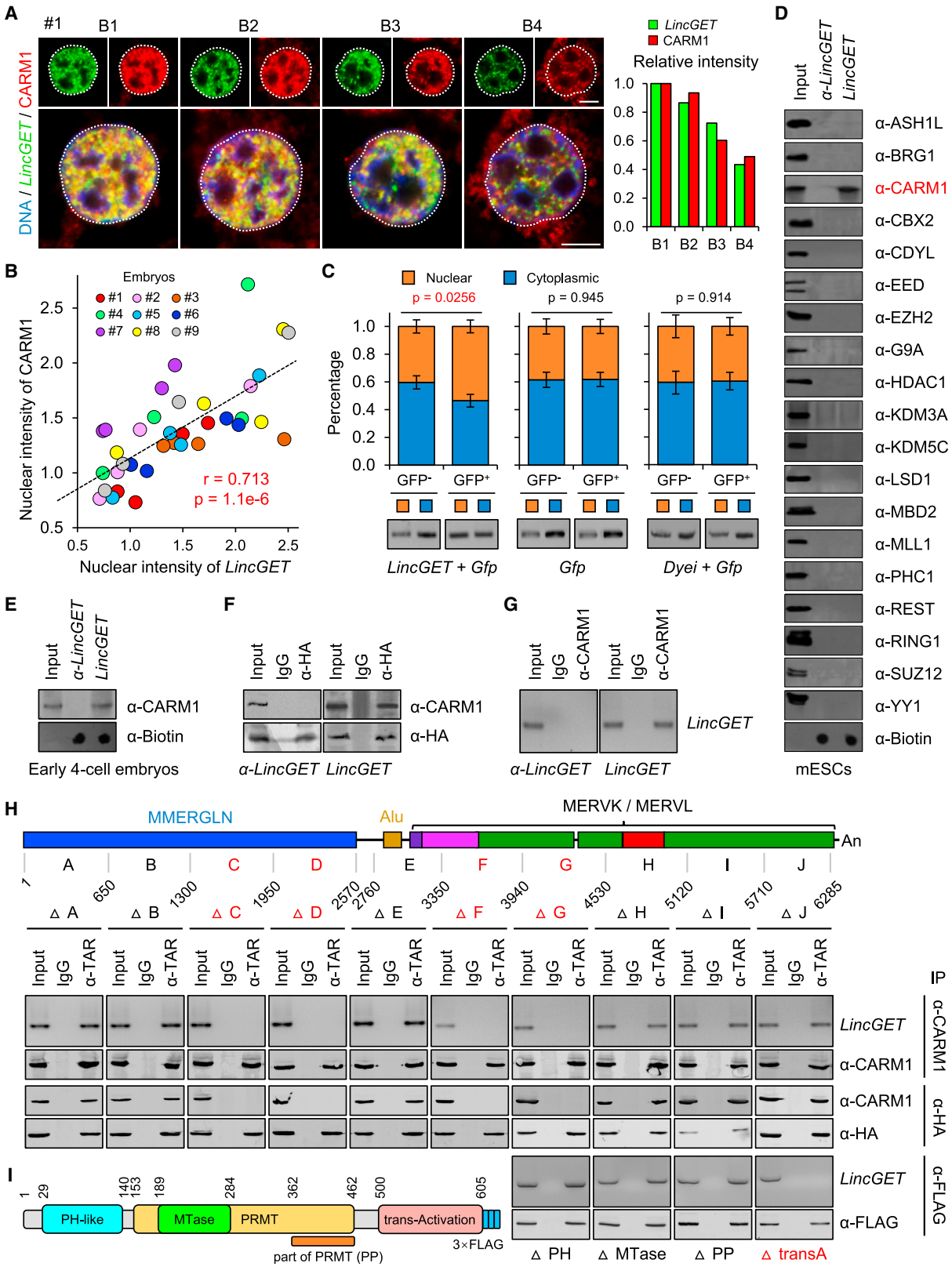

(legend on next page)

next performed RNA pull-down followed by western blotting with biotin-labeled *LincGET* using lysates from mESCs or early four-cell embryos (~2,600 embryos were collected for preparing the lysates for each group). The results showed that *LincGET* prefer to form a complex with CARM1 rather than other well-known epigenetic modifiers such as BRG1, EZH2, G9A, HDAC1, LSD1, SUZ12, and YY1 (Figures 4D and 4E). Moreover, we performed RNA pull-down followed by mass spectrometry using lysates from mESCs and identified 64 *LincGET*-specific binding proteins (*anti-LincGET* as control), which contain CARM1 but no other well-known epigenetic modifiers (Table S4).

Further, we constructed a fused *LincGET-MS2* RNA, whereby a minimal hairpin aptamer (named MS2) was linked to the 5′ end of *LincGET*. The MS2 region of the fused *LincGET-MS2* RNA could selectively bind to dimerized MS2 bacteriophage coat proteins (MS2P) (Peabody, 1993) and thus could be used for coimmunoprecipitation (coIP) experiments. The coIP experiments using mESCs expressing *LincGET-MS2*-fused RNAs and HA-tagged MS2P showed that *LincGET* indeed forms an RNA-protein complex with CARM1 (Figure 4F). Moreover, RNA IP (RIP) of *LincGET* in mESCs transiently overexpressing *LincGET* further confirmed the *LincGET*-CARM1 complex (Figure 4G).

To further identify the functional domain of *LincGET* that interacts with CARM1, we generated a series of truncated *LincGET* RNAs marked with MS2 (Figure 4H) followed by coIP and RIP assays with CARM1. Our data demonstrated that fragments of nucleotides 1,301–2,570 and 3,351–4,530 of *LincGET* were essential for binding to CARM1 (Figure 4H).

We next examined the protein site in CARM1 that interacts with *LincGET*. We constructed four 3 × FLAG-tagged truncated CARM1 mutants with deletion of the pleckstrin homology (PH)-like domain (Δ PH), methyltransferase (MTase) domain (Δ MTase), part of the protein arginine methyltransferase (PRMT) domain (Δ PP), or *trans*-activation domain (Δ transA), respectively. We then performed the RIP assays using mouse epiblast stem cells (mEpiSCs) overexpressing full-length *LincGET* and each of the truncated CARM1 mutants. The results show that the transA domain of CARM1 is essential for *LincGET* binding (Figure 4I).

LincGET/CARM1 Complex Promoted H3R26me2 and Activated ICM Gene Expression

We further examined whether expression of *LincGET* in an early embryo could promote the known events downstream of CARM1, such as the establishment of H3R26me (Torres-Padilla et al., 2007) and expression of genes that promote/represent an ICM fate, such as *Sox2* (Torres-Padilla et al., 2007), *Nanog* (Torres-Padilla et al., 2007), and *Sox21* (Goolam et al., 2016) (Figure 5A). Our results showed that overexpression of *Carm1* or *LincGET* similarly enhanced H3R26me2 levels at the eight-cell stage (Figure 5B) and increased *Nanog*, *Sox2*, and *Sox21* at both RNA and protein levels (Figures 5C–5F). In addition, we found that CDX2 expression at the eight-cell stage was inhibited upon *Carm1* or *LincGET* overexpression (Figure 5G). Notably, the expression level of *Oct4* was not significantly influenced by overexpression of *Carm1* or *LincGET* (Figure S6A). The overall elevated levels of ICM-specific genes in the progeny of *LincGET-*/*Carm1*-overexpressing blastomeres is consistent with and could explain the effect of the *LincGET*/*Carm1* complex in biasing blastomere fate toward ICM.

Given the complex feedback/feedforward nature of ICM fate/pluripotency network, we wonder whether those ICM-specific pluripotent factors overexpression, such as *Nanog*, might also induce *LincGET* expression. As a result, we found *Carm1* overexpression, but not *Nanog* overexpression, would induce *LincGET* expression (Figure S6B).

LincGET/CARM1 Complex Increased Global Chromatin Accessibility

We next explored the potential mechanisms by which the *LincGET*/CARM1 complex activates ICM-specific genes at the

Figure 4. *LincGET* and CARM1 Form a Complex

(A) IF combined with FISH results show *LincGET* and CARM1 co-localization in the nucleus of early four-cell embryos. The intensity analysis of this embryo stage shows that *LincGET* and CARM1 are linearly correlated and different among four blastomeres. The relative intensity of *LincGET*/CARM1 (green/red) to nucleus DNA (blue) was used for comparison, which could reduce errors caused by the depth of the nucleus between blastomeres. Scale bar, 10 μm.

(B) The intensity (relative to DNA signals) analysis of nine embryos shows that *LincGET* and CARM1 are linearly correlated and different among four blastomeres of a four-cell embryo. The correlation coefficient (r) and p value are determined by Pearson's correlation.

(C) CARM1 fractionation analysis showed *LincGET* overexpression, but not *Dyei* or *Gfp* overexpression, increased the percentage of nuclear CARM1. The four-cell embryos, one blastomere of which was injected with *LincGET*/*Gfp* or *Gfp* only at the two-cell stage, were separated into cytoplasmic and nuclear fractions. The CARM1 protein level of each fraction was evaluated by western blotting. More than 400 four-cell embryos were used for each replicate, and three experimental replicates were performed. Isoform abundance on SDS-PAGE gels was measured in ImageJ. Three experimental replicates were performed. The error bars represent SEM. Two-tailed Student's t tests were used for statistical analysis.

(D) RNA pull-down-western blotting using biotinylated *LincGET* or *antisense-LincGET* (*α-LincGET*) with mESCs lysates (left) shows that *LincGET* interacts with CARM1. Three experimental replicates were performed. Two-tailed Student's t tests were used for statistical analysis. α-, anti-.

(E) RNA pull-down western blotting using biotinylated *LincGET* or *antisense-LincGET* (*α-LincGET*) with early four-cell-stage embryo (about 2,600 embryos were used for each experiment) lysates. Three experimental replicates were performed. α-, anti-.

(F) CoIP results using mEpiSCs expressing HA-MS2P with MS2-labeled *LincGET* or *antisense-LincGET* (*α-LincGET*) and anti-HA antibody. The results show that *LincGET* forms an RNA-protein complex with CARM1. Three experimental replicates were performed. α-, anti-.

(G) RIP assays with *LincGET*-expressing mEpiSCs showing that *LincGET* can bind to CARM1. Three experimental replicates were performed. α-, anti-.

(H) CoIP followed by RT-PCR or western blot using mEpiSCs expressing HA-MS2P with MS2-labeled *LincGET* mutants. The results show that the *LincGET* mutants with 1,301–1,950-nt, 1,951–2,570-nt, 3,351–3,940-nt, or 3,941–4,530-nt deletions could not bind CARM1, while other mutants could. Three experimental replicates were performed.

(I) RIP assays with *LincGET*-expressing mEpiSCs expressing *LincGET* and one of the various CARM1 mutants show that the transA domain of CARM1 is essential for binding with *LincGET*. Three experimental replicates were performed. α-, anti-.

See also Figures S4 and S5.

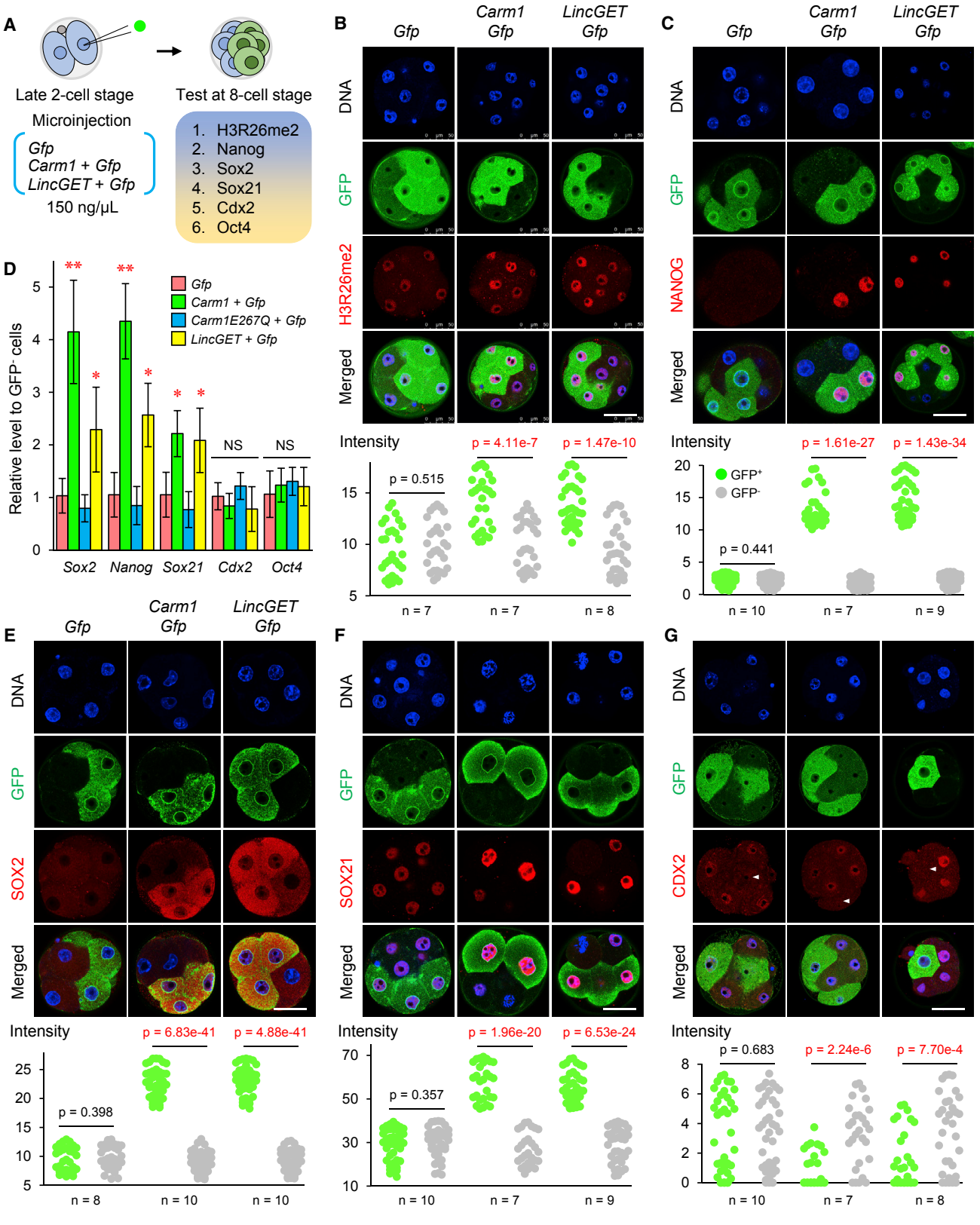

(legend on next page)

eight-cell stage and hypothesized that this may result from altered chromatin accessibility at the promoter regions of these genes. To test this hypothesis, we examined chromatin accessibility by preforming an assay for transposase-accessible chromatin with high-throughput sequencing (ATAC-seq) (Wu et al., 2016). The results showed that the promoters of ICM-specific genes (1,168 genes) (Liu et al., 2016) were more open in *LincGET*- or *Carm1*-overexpressing blastomeres at the eight-cell stage. On the contrary, the chromatin of TE-specific gene (757 genes) (Liu et al., 2016) promoter regions was less open compared to in control blastomeres (Figure 6A).

There is a progressive decrease in chromatin openness along with preimplantation development, which is thought to be important for the transition from totipotency to pluripotency (Bošković et al., 2014). Therefore, we speculated the function of *LincGET*/CARM1 complex in biasing ICM fate might be associated with increasing global chromatin accessibility. To examine chromatin accessibility at the single-cell level, we resorted to an imaging-based *in situ* DNase I-terminal deoxynucleotidyl transferase deoxyuridine triphosphate (dUTP) nick-end labeling (TUNEL) assay (Jachowicz et al., 2017), where the fluorescence intensity observed in TUNEL represents a direct measurement of DNase I sensitivity, and thus chromatin accessibility (Figure 6B). As a result, *LincGET* or CARM1 overexpression similarly led to significantly higher levels of TUNEL fluorescence in the daughter cells of the overexpressed rather than the control blastomeres (Figure 6C). Notably, we did not detect differences in levels of phosphorylated histone H2A.X between the daughter cells of the overexpressed and control blastomeres (Figure 6C), suggesting that the observed increase in DNase I sensitivity was not a result of DNA damage. We also compared nuclear volume, another parameter for chromatin openness (Jachowicz et al., 2017), and observed a significant increase in nuclear volume after *LincGET*/CARM1 overexpression compared to control blastomeres (Figure 6C).

We have reported that *LincGET* prefers to activate genes locating close to long terminal repeats (LTRs) in GLN, MERVL, and ERVK (GLKLTRs) (Wang et al., 2016), and it has been reported that transcriptional activation of transposons such as LINE-1 in early embryos could increase global chromatin accessibility and embryonic pluripotency (Jachowicz et al., 2017). It therefore raised a possibility that *LincGET*/CARM1-mediating ICM-specific genes activation may be linked with transposons activation and global chromatin plasticity. To this end, we indeed found that genomic LINE and LTR sequences are in closer distance to ICM- rather than TE-specific genes (Figure 6D). Besides, the qPCR results indeed showed that overexpression of *LincGET* or *Carm1* in one of the two-cell blastomeres increased the expression level of transposons, including GLN, ERVL, ERVK, and LINE-1 in progeny cells at the eight-cell stage (Figure 6E).

Together, these converging pieces of evidence strongly suggest that *LincGET* and CARM1 bias the blastomeres toward an ICM fate by increasing chromatin openness and activating ICM-specific genes. How the chromatin openness induced by *LincGET*/CARM1 favors gene promoters related to ICM rather than TE remains unclear, but it seems that the *LincGET*/CARM1 complex activates transposons and spreads the active chromatin status toward ICM-specific genes, which prefer to locate near transposons.

Interdependence of *LincGET* and CARM1 in Directing ICM fate

Because *LincGET* could potentially interact with multiple proteins in addition to CARM1, we next examined whether CARM1 was the necessary protein partner that enabled *LincGET* to exert its function regarding the biasing of embryonic fate. By simultaneous overexpression of *LincGET* and depletion of *Carm1* using LNA (Figures S7A and S7B) in one of the two-cell blastomeres, we found that once *Carm1* was knocked down, even if the level of *LincGET* was elevated, the progeny blastomeres were no longer biased toward ICM but rather tended to generate TE (Figures 7A, 7B, S7C, and S7D). Correspondingly, depleting *Carm1* in the *LincGET*-overexpressing blastomeres no longer upregulated the expression of *Sox2*, *Nanog*, and *Sox21*, and, in fact, the H3R26me2 level was decreased (Figures 7C, S7E, and S7F). Also, depleting *Carm1* in the *LincGET*-overexpressing blastomeres was associated with decreased DNase I sensitivity and nuclear volume (Figures 7D, S7G, and S7H), suggesting that the chromatin state became more condensed. These data demonstrated that the function of *LincGET* in biasing embryonic fate requires the presence of CARM1.

To further test whether *LincGET* must interact with CARM1 as a complex to exert its function, we next injected truncated *LincGET* without CARM1-binding sites (nucleotides 1,301–2,570 [ΔC–D] or 3,351–4,530 [ΔF–G]) into one of the two-cell blastomeres with or without knocking down *Carm1*. Compared to the injection of intact *LincGET*, the truncated *LincGET* failed to upregulate *Sox2* and *Sox21* in the progeny blastomeres even in the presence of CARM1 (Figure 7E, red). Besides, the intact *LincGET* could not

Figure 5. *LincGET*/CARM1 Complex Promoted H3R26me and Activated ICM Gene Expression

(A) Schematic overview. RNA (*Gfp*, *Carm1* + *Gfp*, or *LincGET* + *Gfp*) was injected into one blastomere of late two-cell embryos, and the levesl of H3R26me2, *Nanog*, *Sox2*, *Sox21*, *Cdx2*, and *Oct4* were tested at eight-cell stage.

(B) H3R26me2 staining of eight-cell embryos shows that *Carm1* or *LincGET* overexpression led to a dramatic increase in H3R26me2 modification. For fluorescence analysis, the green ball stands for GFP^+ cells, and the gray ball stands for GFP^- cells. Three experimental replicates were performed. Scale bar, 50 μm. Two-tailed Student's t tests were used for statistical analysis.

(C–F) NANOG (C), SOX2 (E), and SOX21 (F) were increased in the progeny of *Carm1*- or *LincGET*-injected blastomeres at both the RNA (D) and protein levels. The group names in (F) are the same as in (B); the group names in (G) are the same as in (C). Three experimental replicates were performed. Scale bar, 50 μm. The error bars represent SEM. For fluorescence analysis, the green ball stands for GFP^+ cells and the gray ball stands for GFP^- cells. Two-tailed Student's t tests were used for statistical analysis. Compared to the *Gfp* group, $^{**}p < 0.001$, $^{*}0.01 < p < 0.05$ (not significant [NS]), $p > 0.05$.

(G) No change in CDX2 was found in the progeny of *Carm1*- or *LincGET*-injected blastomeres. Interestingly, CDX2 was detected in only some blastomeres (blastomeres showing no CDX2 expression are marked with white arrowheads). Three experimental replicates were performed. Scale bar, 50 μm. For fluorescence analysis, the green ball stands for GFP^+ cells, and the gray ball stands for GFP^- cells. Two-tailed Student's t tests were used for statistical analysis. See also Figure S6.

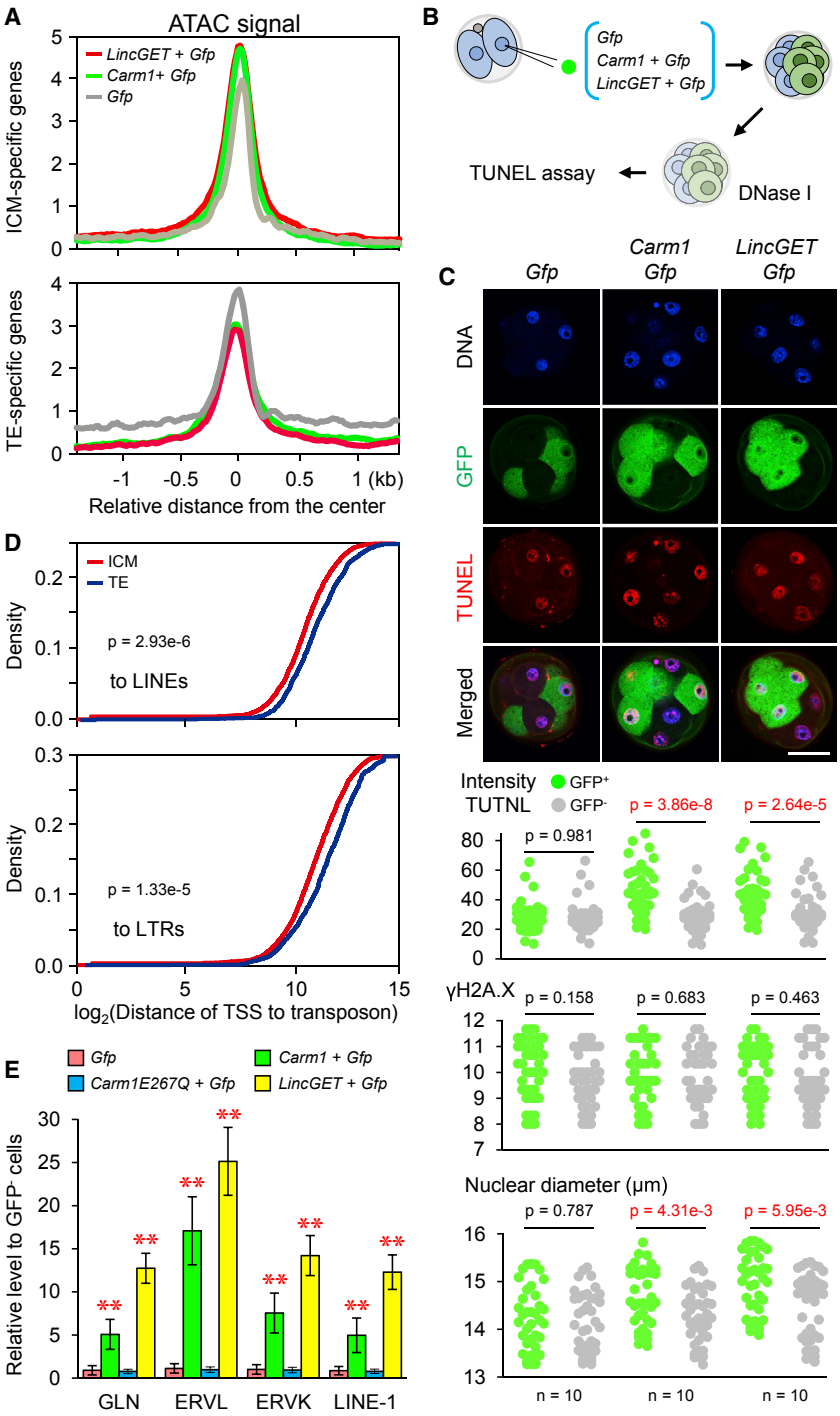

Figure 6. *LincGET*/CARM1 Increased Global Chromatin Accessibility

(A) ATAC-seq results show that the promoters of ICM-specific genes are more open in *LincGET*- or *Carm1*-overexpressing blastomeres, while the chromatin of TE-specific promoter regions is less open compared to in the control blastomeres.

(B) Overview of DNase I-TUNEL assay.

(C) *LincGET* or CARM1 overexpression led to significantly higher levels of TUNEL fluorescence and increased nuclear volume in daughter cells of injected blastomeres. Scale bar, 50 μm. Three experimental replicates were performed. For fluorescence analysis, the green ball stands for GFP^+ cells, and the gray ball stands for GFP^- cells. Two-tailed Student's t tests were used for statistical analysis.

(D) Bioinformatic analysis revealed that genomic LINE or LTR sequences are in closer distance to ICM-specific genes rather than TE-specific genes. Two-sample Kolmogorov-Smirnov tests were used for statistical analysis.

(E) qPCR shows that overexpression of *LincGET* or *Carm1* increased the expression level of transposons such as GLN, ERVL, ERVK, and LINE-1. Three experimental replicates were performed. The error bars represent SEM. Two-tailed Student's t tests were used for statistical analysis. $^{**}p < 0.01$.

upregulate either *Sox2* or *Sox21* when *Carm1* was depleted (Figures 7E and 7F, orange). These results indicated the functional necessity of the *LincGET*-CARM1 complex.

In addition, we found that depletion of *LincGET* led to late two-cell-stage arrest (10 μM LNA with nearly 100% interference efficiency), which could not be rescued by *Carm1* overexpression (Figure S7I), suggesting that *LincGET* is a master regulator upstream of Carm1 and that it may have other essential functions beyond interaction with *CARM1*.

Functional Domain of *LincGET* beyond CARM1 Binding

During our functional screening of truncated *LincGET* mutants, overexpression of several truncated *LincGET* mutants (Δ 2,761–3,350 [ΔE] or Δ 5,121–5,710 [ΔI]) in early-stage embryos led to binding to CARM1 but failed to upregulate *Sox2* and *Sox21* (Figure 7F, green). This suggested that these truncated regions harbor important functional domains. By overexpressing both CARM1 and these *LincGET* mutants, we found that the truncated *LincGET* mutants exerted a dominant-negative effect in cancelling CARM1's function regarding upregulating *Sox2* and *Sox21* (Figure 7G, green). We propose that these functional domains of *LincGET* might be acting as "anchors" to guide the *LincGET*-CARM1 complex to its correct location in the nucleus, without which CARM1 could not function normally event if the *LincGET*-CARM1 complex was formed (Figure 7H).

DISCUSSION

The mechanisms of early mammalian cell fate determination remain to be elucidated due to the multiple layers of regulation.

A

Group	Blastocysts 3D (%)	Total cells (n)	Inner cells (%)	GFP cells (%)	Inner cells that are GFP+ (%)	GFP cells that are inner (%)
Gfp	65 (82.65)	41.91 ± 8.79	(37.68 ± 3.43)	(49.02 ± 3.44)	(53.06 ± 8.03) [x]	(40.51 ± 4.60) [x]
LincGET + i-*Carm1* + *Gfp*	62 (85.18)	41.85 ± 8.75	(36.20 ± 3.86)	(46.20 ± 5.75)	(43.06 ± 12.70) [y]	(32.89 ± 6.02) [y]

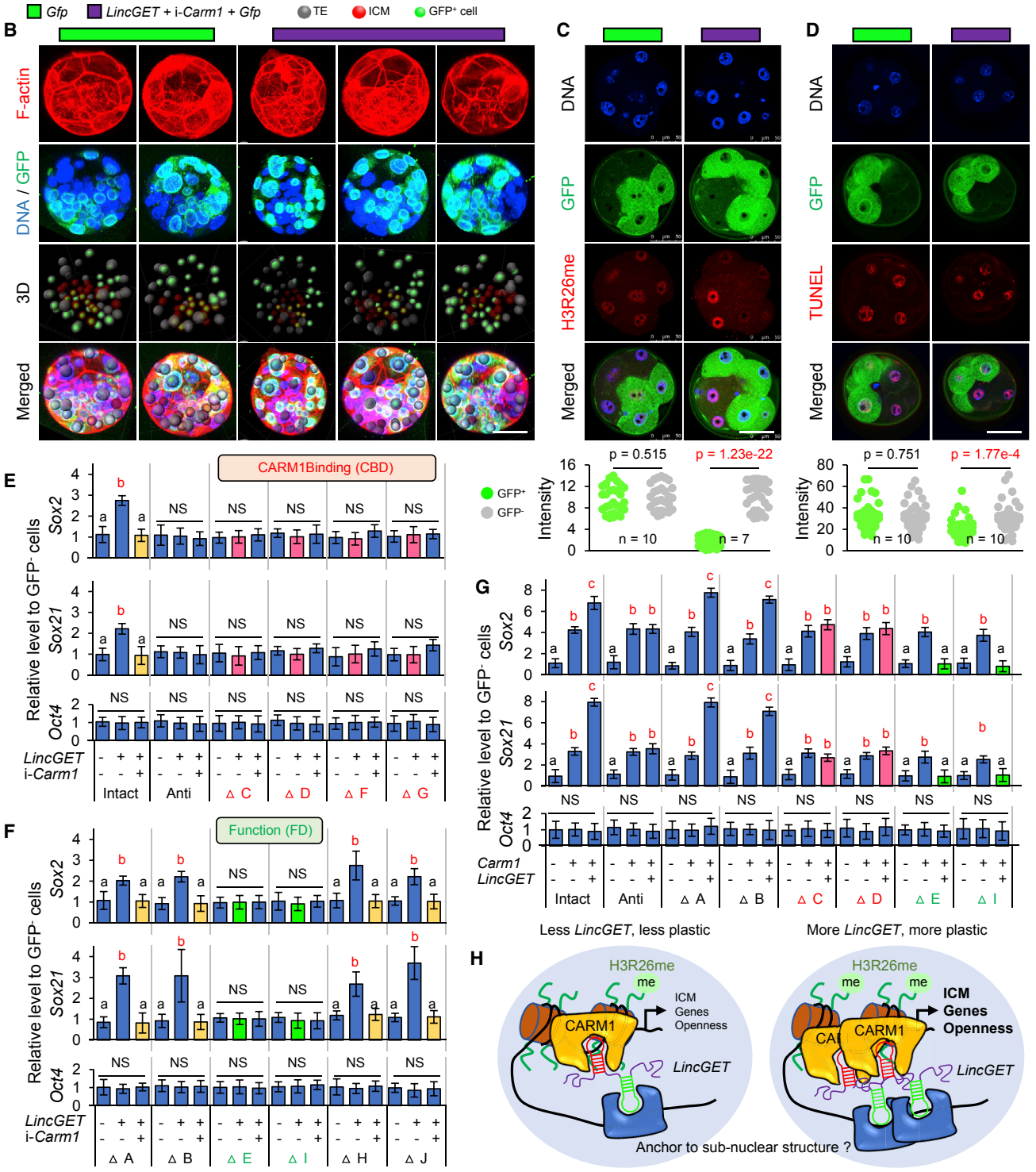

(legend on next page)

It remains debatable whether early blastomeres are equal in their developmental fate until the 16-cell stage or whether certain developmental bias already exists before the eight-cell stage, which predisposes early blastomeres toward either an ICM or a TE fate (Wennekamp et al., 2013; Zernicka-Goetz et al., 2009). Recent research advances have documented the molecular differences between early mammalian blastomeres as early as the four-cell stage. Epigenetic/genetic regulators such as CARM1/PRDM14, H3R26 methylation, DNA-binding dynamics of SOX2 or OCT4, and the level of SOX21 have shown heterogeneity between four-cell blastomeres to bias cell fate (Goolam et al., 2016; Piotrowska-Nitsche et al., 2005; Plachta et al., 2011; Tabansky et al., 2013; Torres-Padilla et al., 2007; White et al., 2016). However, the origin of the molecular heterogeneity observed at the four-cell stage remains an unresolved issue. Our data provide further evidence that the heterogeneous expression of *LincGET* at the late two-cell stage could act as an upstream regulator to influence subsequent lineage fate.

In fact, although two-cell blastomeres are generally considered to be totipotent, there are previous pieces of evidence and recent emerging reports showing that when two-cell blastomeres are separated, in the majority of cases, only one of the two-cell blastomeres develops into a mouse (Casser et al., 2017; Katayama et al., 2010; Morris et al., 2012; Papaioannou and Ebert, 1995; Tsunoda and McLaren, 1983). These data demonstrate inequality in the totipotency of two-cell blastomeres. Thus, our data regarding the heterogeneity of *LincGET* and its function in biasing lineage fate provide a molecular explanation for those experimental observations. The expression level of *LincGET* at the early two-cell embryo stage is almost absent, but it increases robustly at the late two-cell stage and shows heterogeneous expression between two-cell blastomeres (Figures 1 and S1). This suggests that the observed heterogeneity at the late two-cell embryo stage is generated *de novo* and thus may represent the gene expression noise that inevitably rises during ZGA, as previously reported (Shi et al., 2015). Alternatively, the heterogeneity of *LincGET* at the late two-cell stage may be triggered by unequally distributed unknown factors that already existed in the early two-cell embryos.

Early cleavage embryos are known to harbor many active ERVs, yet little is known about their functions (Evsikov et al., 2004; Peaston et al., 2004). It has been reported that MERVL transcription is a unique marker of two-cell mouse embryos and two-cell-like mESCs, which have higher pluripotency than that of normal mESCs (Macfarlan et al., 2012). In addition, embryonic chromatin at the two-cell stage has high core-histone mobility, and embryonic chromatin becomes progressively more compacted, losing plasticity and decreased developmental potency from totipotency to pluripotency (Bošković et al., 2014; Jachowicz et al., 2017). Active ERVs at the cleavage stage may have key roles in establishing totipotency to prepare materials for both TE and ICM lineage determination. There are numerous copies of ERV in the genome, which may provide an advantage for global chromatin opening. *LincGET* is a GLN-, MERVL-, and ERVK-associated lincRNA, and we found that increased *LincGET* expression enables ICM-specific gene promoters to become more open (Figure 6A). The origin of *LincGET* remains unknown, yet it raises the possibility that there might be other lncRNAs that are heavily associated with transposable elements that play important roles in early embryo development. In addition, we further propose that differential ERV activation resulting from ZGA may generate asymmetric patterns between two blastomeres, similar to *LincGET*, and thus may provide an additional resource for biasing embryonic fate.

As a recently identified lncRNA, we previously revealed the role of *LincGET* in controlling alternative splicing (Wang et al.,

Figure 7. Interdependence of *LincGET* and CARM1 in Directing ICM Fate

(A) The distribution of progeny of injected blastomere at the blastocyst stage based on 3D reconstruction analysis. Two-tailed Student's t tests were used for statistical analysis. Different letters between x and y indicate very significant differences ($p < 0.00001$). Key to table headings: blastocyst 3D (%) is the number and developmental rate of blastocysts that were all used for 3D analysis, total cells is the total number of cells in the blastocyst, inner cells (%) is the percentage of inner cells out of the total number of cells in the blastocyst, GFP cells (%) is the percentage of GFP-positive cells out of the total number of cells in the blastocyst, GFP cells that are inner (%) is the percentage of GFP-positive inner cells out of the total number of GFP-positive cells in the blastocyst, and inner cells that are GFP^+ (%) is the percentage of GFP-positive inner cells out of the total number of inner cells in the blastocyst.

(B) Examples of 3D analysis results. Scale bar, 50 μm.

(C) H3R26me2 staining shows that interference with *Carm1* could reduce H3R26me2 levels even in the presence of *LincGET* overexpression. Three experimental replicates were performed. For fluorescence analysis, the green ball stands for GFP^+ cells, and the gray ball stands for GFP^- cells. Two-tailed Student's t tests were used for statistical analysis. Scale bar, 50 μm.

(D) TUNEL fluorescent assay shows significantly lower levels of TUNEL fluorescence in daughter cells of *LincGET*-overexpressing and *Carm1*-depleted blastomeres. Three experimental replicates were performed. For fluorescence analysis, the green ball stands for GFP^+ cells, and the gray ball stands for GFP^- cells. Two-tailed Student's t tests were used for statistical analysis. Scale bar, 50 μm.

(E) qPCR results show that the truncated *LincGET* without CARM1 binding sites (Δ1,301–2,570 [ΔC–D] or Δ3,351–4,530 [ΔF–G]) failed to upregulate *Sox2* and *Sox21* in progeny blastomeres (red), and the intact *LincGET* exhibited no transcriptional activation activity when *Carm1* was depleted (orange). Three experimental replicates were performed. The error bars represent SEM. Two-tailed Student's t tests were used for statistical analysis. Different letters (a or b) indicate $p < 0.05$ (NS), $p > 0.05$.

(F) qPCR results show that some truncated *LincGET* mutants exhibited no transcriptional activation activity when *Carm1* was depleted (orange), and several truncated *LincGET* mutants (Δ 2,761–3,350 [ΔE] or Δ 5,121–5,710 [ΔI]) could bind to CARM1 but failed to upregulate *Sox2* and *Sox21* (green). Three experimental replicates were performed. The error bars represent SEM. Two-tailed Student's t tests were used for statistical analysis. Different letters (a or b) indicate $p < 0.05$ (NS), $p > 0.05$.

(G) qPCR results show that upregulation of *Sox2* and *Sox21* upon CARM1 overexpression could be cancelled by truncated *LincGET* (Δ 2,761–3,350 [ΔE] or Δ 5,121–5,710 [ΔI]). Three experimental replicates were performed. The error bars represent SEM. Two-tailed Student's t tests were used for the statistical analysis. Different letters (a, b, or c) indicate $p < 0.05$ (NS), $p > 0.05$.

(H) ICM bias model of the *LincGET*-CARM1 complex.

See also Figure S7 and Table S2.

2016). In addition to this mechanism, here, we further found that *LincGET* could upregulate *Sox2* and *Sox21* by forming a complex with CARM1, mostly in the nucleus. This supported the idea that in addition to the expression level, the intracellular location of the RNA/protein is essential in exerting proper functions. LncRNAs have emerged as key components of intracellular scaffolds that allow proper assembly of protein complexes, genes, and chromosomes subject to proper activation and deactivation (Batista and Chang, 2013). Intriguingly, another well-characterized lncRNA, *Neat1*, is also associated with transposable elements and is essential for the formation of a specific nuclear body structure called paraspeckle (Clemson et al., 2009; Lin et al., 2018). *LincGET* may function in a similar fashion to *Neat1* in terms of forming a scaffold and an "address code" for recruiting diffusible CARM1 and other essential proteins in the nucleus. Truncated *LincGET* (Δ2,761–3,350 [ΔE] or Δ 5,121–5,710 [ΔI]) could bind to CARM1 but failed to activate CARM1 target gene expression, and this may be due to the disruption of the scaffold region of *LincGET* that is essential for anchoring the complex to the correct intranuclear "address."

STAR★METHODS

Detailed methods are provided in the online version of this paper and include the following:

- KEY RESOURCES TABLE
- CONTACT FOR REAGENT AND RESOURCE SHARING
- EXPERIMENTAL MODEL AND SUBJECT DETAILS
  - Mouse embryos collection
  - Culture Cells
- METHOD DETAILS
  - RT-qPCR and 1C-qPCR
  - Plasmid vectors construction
  - CARM1 fractionation
  - Micro-injection
  - RNA pull-down
  - Western blotting
  - Mass spectrometry
  - Immunoprecipitation
  - Northern blotting
  - Immunofluorescence staining
  - RNA-FISH and IF combining RNA-FISH
  - Microscopic analysis and three-dimensional reconstructions
  - In vivo DNase I TUNEL assay
  - ATAC-seq library preparation and bioinformatic analyses of expression and heterogeneity in early embryo
- QUANTIFICATION AND STATISTICAL ANALYSIS
- DATA AND SOFTWARE AVAILABILITY
  - Data Resources

SUPPLEMENTAL INFORMATION

Supplemental Information includes seven figures and five tables and can be found with this article online at https://doi.org/10.1016/j.cell.2018.11.039.

ACKNOWLEDGMENTS

We thank Shiwen Li and Xili Zhu from the Institute of Zoology, Chinese Academy of Sciences, and Bofeng Liu, Wei Xie, and Yingying Gao from Tsinghua University for their technical assistance. This work was supported by grants from the Strategic Priority Research Program of the Chinese Academy of Sciences (XDA16030400 to Q.Z. and W.L.), National Natural Science Foundation of China (31621004 to Q.Z. and W.L., 31471395 to Q.Z.), the Key Research Projects of the Frontier Science of the Chinese Academy of Sciences (QYZDY-SSW-SMC002 to Q.Z.), the Key Deployment Projects of the Chinese Academy of Sciences (QYZDB-SSW-SMC022 to W.L.), the China Postdoctoral Science Foundation (2017M610990 and 2017T100107 to J.W.), the China National Postdoctoral Program for Innovative Talents (BX201700243 to L.W.), and the National Key Research and Development Program (2017YFA0103803 to Q.Z.).

AUTHOR CONTRIBUTIONS

J.W., W.L., and Q.Z. conceived and designed the study. J.W., L.W., G.F., Y.W., Y.L., X.L., C.L., G.J., and C.H. performed the experiments. J.W., L.W., G.F., J.S., T.Z., Q.C., Z.L., W.L., and Q.Z. analyzed the data. W.L. and Q.Z. supervised the project. J.W., G.F., Q.C., W.L., and Q.Z. designed and wrote the manuscript.

DECLARATION OF INTERESTS

The authors declare no competing interests.

Received: March 22, 2018
Revised: July 1, 2018
Accepted: November 22, 2018
Published: December 13, 2018

REFERENCES

Batista, P.J., and Chang, H.Y. (2013). Long noncoding RNAs: cellular address codes in development and disease. Cell *152*, 1298–1307.

Bošković, A., Eid, A., Pontabry, J., Ishiuchi, T., Spiegelhalter, C., Raghu Ram, E.V., Meshorer, E., and Torres-Padilla, M.E. (2014). Higher chromatin mobility supports totipotency and precedes pluripotency in vivo. Genes Dev. *28*, 1042–1047.

Burton, A., Muller, J., Tu, S., Padilla-Longoria, P., Guccione, E., and Torres-Padilla, M.E. (2013). Single-cell profiling of epigenetic modifiers identifies PRDM14 as an inducer of cell fate in the mammalian embryo. Cell Rep. *5*, 687–701.

Casser, E., Israel, S., Witten, A., Schulte, K., Schlatt, S., Nordhoff, V., and Boiani, M. (2017). Totipotency segregates between the sister blastomeres of two-cell stage mouse embryos. Sci. Rep. *7*, 8299.

Clemson, C.M., Hutchinson, J.N., Sara, S.A., Ensminger, A.W., Fox, A.H., Chess, A., and Lawrence, J.B. (2009). An architectural role for a nuclear noncoding RNA: NEAT1 RNA is essential for the structure of paraspeckles. Mol. Cell *33*, 717–726.

Deng, Q., Ramskold, D., Reinius, B., and Sandberg, R. (2014). Single-cell RNA-seq reveals dynamic, random monoallelic gene expression in mammalian cells. Science *343*, 193–196.

Evsikov, A.V., de Vries, W.N., Peaston, A.E., Radford, E.E., Fancher, K.S., Chen, F.H., Blake, J.A., Bult, C.J., Latham, K.E., Solter, D., and Knowles, B.B. (2004). Systems biology of the 2-cell mouse embryo. Cytogenet. Genome Res. *105*, 240–250.

Goolam, M., Scialdone, A., Graham, S.J.L., Macaulay, I.C., Jedrusik, A., Hupalowska, A., Voet, T., Marioni, J.C., and Zernicka-Goetz, M. (2016). Heterogeneity in Oct4 and Sox2 Targets Biases Cell Fate in 4-Cell Mouse Embryos. Cell *165*, 61–74.

Guttman, M., Donaghey, J., Carey, B.W., Garber, M., Grenier, J.K., Munson, G., Young, G., Lucas, A.B., Ach, R., Bruhn, L., et al. (2011). lincRNAs act in the circuitry controlling pluripotency and differentiation. Nature *477*, 295–300.

Hamazaki, N., Uesaka, M., Nakashima, K., Agata, K., and Imamura, T. (2015). Gene activation-associated long noncoding RNAs function in mouse preimplantation development. Development *142*, 910–920.

Hu, W., Alvarez-Dominguez, J.R., and Lodish, H.F. (2012). Regulation of mammalian cell differentiation by long non-coding RNAs. EMBO Rep. *13*, 971–983.

Jachowicz, J.W., Bing, X., Pontabry, J., Bošković, A., Rando, O.J., and Torres-Padilla, M.E. (2017). LINE-1 activation after fertilization regulates global chromatin accessibility in the early mouse embryo. Nat. Genet. *49*, 1502–1510.

Katayama, M., Ellersieck, M.R., and Roberts, R.M. (2010). Development of monozygotic twin mouse embryos from the time of blastomere separation at the two-cell stage to blastocyst. Biol. Reprod. *82*, 1237–1247.

Langmead, B., and Salzberg, S.L. (2012). Fast gapped-read alignment with Bowtie 2. Nat. Methods *9*, 357–359.

Lin, Y., Schmidt, B.F., Bruchez, M.P., and McManus, C.J. (2018). Structural analyses of NEAT1 lncRNAs suggest long-range RNA interactions that may contribute to paraspeckle architecture. Nucleic Acids Res. *46*, 3742–3752.

Liu, W., Liu, X., Wang, C., Gao, Y., Gao, R., Kou, X., Zhao, Y., Li, J., Wu, Y., Xiu, W., et al. (2016). Identification of key factors conquering developmental arrest of somatic cell cloned embryos by combining embryo biopsy and single-cell sequencing. Cell Discov. *2*, 16010.

Macfarlan, T.S., Gifford, W.D., Driscoll, S., Lettieri, K., Rowe, H.M., Bonanomi, D., Firth, A., Singer, O., Trono, D., and Pfaff, S.L. (2012). Embryonic stem cell potency fluctuates with endogenous retrovirus activity. Nature *487*, 57–63.

Morris, S.A., Guo, Y., and Zernicka-Goetz, M. (2012). Developmental plasticity is bound by pluripotency and the Fgf and Wnt signaling pathways. Cell Rep. *2*, 756–765.

Namekawa, S.H., and Lee, J.T. (2011). Detection of nascent RNA, single-copy DNA and protein localization by immunoFISH in mouse germ cells and preimplantation embryos. Nat. Protoc. *6*, 270–284.

Ng, S.Y., and Stanton, L.W. (2013). Long non-coding RNAs in stem cell pluripotency. Wiley Interdiscip. Rev. RNA *4*, 121–128.

Papaioannou, V.E., and Ebert, K.M. (1995). Mouse half embryos: viability and allocation of cells in the blastocyst. Dev. Dyn. *203*, 393–398.

Peabody, D.S. (1993). The RNA binding site of bacteriophage MS2 coat protein. EMBO J. *12*, 595–600.

Peaston, A.E., Evsikov, A.V., Graber, J.H., de Vries, W.N., Holbrook, A.E., Solter, D., and Knowles, B.B. (2004). Retrotransposons regulate host genes in mouse oocytes and preimplantation embryos. Dev. Cell *7*, 597–606.

Piotrowska-Nitsche, K., Perea-Gomez, A., Haraguchi, S., and Zernicka-Goetz, M. (2005). Four-cell stage mouse blastomeres have different developmental properties. Development *132*, 479–490.

Plachta, N., Bollenbach, T., Pease, S., Fraser, S.E., and Pantazis, P. (2011). Oct4 kinetics predict cell lineage patterning in the early mammalian embryo. Nat. Cell Biol. *13*, 117–123.

Rinn, J.L., and Chang, H.Y. (2012). Genome regulation by long noncoding RNAs. Annu. Rev. Biochem. *81*, 145–166.

Rossant, J., and Tam, P.P. (2009). Blastocyst lineage formation, early embryonic asymmetries and axis patterning in the mouse. Development *136*, 701–713.

Shi, J., Chen, Q., Li, X., Zheng, X., Zhang, Y., Qiao, J., Tang, F., Tao, Y., Zhou, Q., and Duan, E. (2015). Dynamic transcriptional symmetry-breaking in pre-implantation mammalian embryo development revealed by single-cell RNA-seq. Development *142*, 3468–3477.

Shin, H., Liu, T., Manrai, A.K., and Liu, X.S. (2009). CEAS: cis-regulatory element annotation system. Bioinformatics *25*, 2605–2606.

Shuai, L., Wang, Y., Dong, M., Wang, X., Sang, L., Wang, M., Wan, H., Luo, G., Gu, T., Yuan, Y., et al. (2015). Durable pluripotency and haploidy in epiblast stem cells derived from haploid embryonic stem cells in vitro. J. Mol. Cell Biol. *7*, 326–337.

Tabansky, I., Lenarcic, A., Draft, R.W., Loulier, K., Keskin, D.B., Rosains, J., Rivera-Feliciano, J., Lichtman, J.W., Livet, J., Stern, J.N., et al. (2013). Developmental bias in cleavage-stage mouse blastomeres. Curr. Biol. *23*, 21–31.

Torres-Padilla, M.E., Parfitt, D.E., Kouzarides, T., and Zernicka-Goetz, M. (2007). Histone arginine methylation regulates pluripotency in the early mouse embryo. Nature *445*, 214–218.

Tsunoda, Y., and McLaren, A. (1983). Effect of various procedures on the viability of mouse embryos containing half the normal number of blastomeres. J. Reprod. Fertil. *69*, 315–322.

Wang, J., Li, X., Wang, L., Li, J., Zhao, Y., Bou, G., Li, Y., Jiao, G., Shen, X., Wei, R., et al. (2016). A novel long intergenic noncoding RNA indispensable for the cleavage of mouse two-cell embryos. EMBO Rep. *17*, 1452–1470.

Wennekamp, S., Mesecke, S., Nédélec, F., and Hiiragi, T. (2013). A self-organization framework for symmetry breaking in the mammalian embryo. Nat. Rev. Mol. Cell Biol. *14*, 452–459.

White, M.D., Angiolini, J.F., Alvarez, Y.D., Kaur, G., Zhao, Z.W., Mocskos, E., Bruno, L., Bissiere, S., Levi, V., and Plachta, N. (2016). Long-Lived Binding of Sox2 to DNA Predicts Cell Fate in the Four-Cell Mouse Embryo. Cell *165*, 75–87.

Wu, J., Huang, B., Chen, H., Yin, Q., Liu, Y., Xiang, Y., Zhang, B., Liu, B., Wang, Q., Xia, W., et al. (2016). The landscape of accessible chromatin in mammalian preimplantation embryos. Nature *534*, 652–657.

Zernicka-Goetz, M., Morris, S.A., and Bruce, A.W. (2009). Making a firm decision: multifaceted regulation of cell fate in the early mouse embryo. Nat. Rev. Genet. *10*, 467–477.

Zhang, Y., Liu, T., Meyer, C.A., Eeckhoute, J., Johnson, D.S., Bernstein, B.E., Nusbaum, C., Myers, R.M., Brown, M., Li, W., and Liu, X.S. (2008). Model-based analysis of ChIP-Seq (MACS). Genome Biol. *9*, R137.

STAR★METHODS

KEY RESOURCES TABLE

REAGENT or RESOURCE	SOURCE	IDENTIFIER
Antibodies		
Mouse monoclonal anti-FLAG	Sigma	Cat# F1804; RRID: AB_262044
Mouse monoclonal anti-CARM1	Santa Cruz	Cat# sc-393381; RRID: AB_2732840
Rat monoclonal anti-Tubulin	Abcam	Cat# ab6160; RRID: AB_305328
Chicken polyclonal anti-GFP	Abcam	Cat# ab13970; RRID: AB_300798
Goat polyclonal anti-SOX2	Santa Cruz	Cat# sc-17319; RRID: AB_661259
Mouse monoclonal anti-ASHL1	Abcam	Cat# ab50981; RRID: AB_867738
Rabbit polyclonal anti-BRG1	Abcam	Cat# ab4081; RRID: AB_304271
Rabbit polyclonal anti-CBX2	Abcam	Cat# ab80044; RRID: AB_2049270
Rabbit polyclonal anti-CDYL	Abcam	Cat# ab5188; RRID: AB_304770
Rabbit polyclonal anti-EED	Abcam	Cat# ab4469; RRID: AB_2262066
Rabbit polyclonal anti-EZH2	Abcam	Cat# ab186006; RRID: AB_2661845
Rabbit polyclonal anti-G9A	Abcam	Cat# ab40542; RRID: AB_731483
Rabbit polyclonal anti-HDAC1	Abcam	Cat# ab7028; RRID: AB_305705
Rabbit monoclonal anti-KDM3A	Abcam	Cat# ab91252; RRID: AB_2049835
Rabbit polyclonal anti-KDM5C	Abcam	Cat# ab34718; RRID: AB_881090
Rabbit polyclonal anti-LSD1	Abcam	Cat# ab17721; RRID: AB_443964
Rabbit polyclonal anti-MBD2	Abcam	Cat# ab38646; RRID: AB_2139612
Mouse monoclonal anti-MLL1	Abcam	Cat# ab32400; RRID: AB_1269267
Mouse polyclonal anti-PHC1	Abcam	Cat# ab52674; RRID: AB_2042623
Rabbit polyclonal anti-REST	Abcam	Cat# ab21635; RRID: AB_777678
Rabbit polyclonal anti-RING1A	Abcam	Cat# ab32644; RRID: AB_2238272
Rabbit polyclonal anti-SUZ12	Abcam	Cat# ab12073; RRID: AB_442939
Rabbit monoclonal anti-YY1	Abcam	Cat# ab109237; RRID: AB_10890662
Rabbit polyclonal anti-Biotin	Abcam	Cat# ab1227; RRID: AB_298990
Rabbit polyclonal anti-HA	Abcam	Cat# ab9110; RRID: AB_307019
Rabbit polyclonal anti-H3R26me2	Abcam	Cat# ab127095; RRID: AB_2732841
Goat polyclonal anti-NANOG	Santa Cruz	Cat# sc-30329; RRID: AB_2150123
Rabbit polyclonal anti-SOX21	Biorbyt	Cat# orb158458; RRID: AB_2732842
Rabbit monoclonal anti-CDX2	Abcam	Cat# ab76541; RRID: AB_1523334
Goat polyclonal anti-OCT4	Abcam	Cat# sc-8629; RRID: AB_2167705
Rabbit polyclonal anti-γH2A.X	Abcam	Cat# ab2893; RRID: AB_303388
Chemicals, Peptides, and Recombinant Proteins		
PMSG	ProSpec	Cat# HOR-272
hCG	ProSpec	Cat# HOR-250
ChromaTide Alexa Fluor 488-5-UTP	Invitrogen	Cat# C11403
Formamide	Sigma	Cat# F9037
Dextran Sulfate	Sigma	Cat# 30915
20 × SSC	Sigma	Cat# S6639-1L
Triton X-100	Sigma	Cat# T8787-50ML
Vanadyl ribonucleoside complex	Sigma	Cat# 94742-1ML
VECTASHIELD with DAPI	Vector	Cat# H1200
Ribonuclease Inhibitor	Invitrogen	Cat# 10777019
Pronase	Sigma	Cat# P8811

(*Continued on next page*)

Continued

REAGENT or RESOURCE	SOURCE	IDENTIFIER
Cas9 protein	PNA Bio	Cat# CP02-50
Ambion Recombinant RNase A	Ambion	Cat# AM2269
bFGF	R&D	Cat# 233-FB-001MG/CF
Activin A	R&D	Cat# 338-AC-01M
0.05% trypsin/EDTA	GIBCO	Cat# 25300062
Pierce IP Lysis Buffer	Pierce	Cat# 87787
Protease Inhibitor Cocktail	Pierce	Cat# 78441
Critical Commercial Assays		
RNeasy Mini Kit	QIAGEN	Cat# 74104
RNase-Free DNase Set	QIAGEN	Cat# 79254
High Capacity cDNA Reverse Transcription Kit	ABI	Cat# 4368814
Power SYBR Green PCR Master Mix	ABI	Cat# 4367659
TaqMan Universal Master Mix II	Life	Cat# 4440048
Single Cell-to-CT™ qRT-PCR Kit	Invitrogen	Cat# 4458237
LongAmpTM *Taq* DNA Polymerase	NEB	Cat# M0534L
mMESSAGEmMACHINE T7 ULTRA Kit	Ambion	Cat# AMB1345-5
MEGAshortscript™ Kit	Ambion	Cat# AM1354
Pierce RNA 3′ End Desthiobiotinylation Kit	Pierce	Cat# 20163
Pierce Magnetic RNA-Protein Pull-Down Kit	Pierce	Cat# 20164
Magna RIP Kit	Millipore	Cat# 17-700
Click-iT TUNEL Alexa Fluor Imaging Assay Kit	Life	Cat# C10247
TruePrepTM DNA Library Prep Kit V2 for Illumina	Vazyme	Cat# TD502
DIG detection kit	Roche	Cat# 11093657910
AMPure XP Product	Backman	Cat# A63880
Lipofectamine 3000 transfection reagent	GIBCO	Cat# L3000015
Deposited Data		
ATAC-seq	This Paper	GEO: GSE110419
DOI for our Mendeley dataset	This Paper	https://doi.org/10.17632/vc5tv49rdf.1
Experimental Models: Cell Lines		
Mouse embryonic stem cells (mESCs)	This Paper	Established in our lab
Mouse epiblast stem cells (mEpiSCs)	This Paper	Established in our lab
Experimental Models: Organisms/Strains		
ICR strain mice		Bought from Charles River
Oligonucleotides		
see Table S5		N/A
Recombinant DNA		
pEASY-T3	TransGen	Cat# CT301-02
pEASY-T3-LincGET(2574-2763)	This Paper	PCR & TA cloning
pEASY-T3-Dyei(384-642)	This Paper	PCR & TA cloning
pEASY-T3-GFP(362-668)	This Paper	PCR & TA cloning
pEASY-T3-Dyei	This Paper	PCR & TA cloning
pUC57-T7-GFP_KASH	BGI	Gene synthesized by BGI company
pCMV-T7-CARM1(NM_021531)	YouBio	Bought from YouBio company
pCMV-T7-CARM1(NM_153141)	YouBio	Bought from YouBio company
pCMV-T7-CARM1E267Q(NM_021531)	This Paper	Mutant from pCMV-T7-CARM1 (NM_021531)
pCMV-T7-CARM1E267Q(NM_153141)	This Paper	Mutant from pCMV-T7-CARM1 (NM_153141)

(*Continued on next page*)

Continued

REAGENT or RESOURCE	SOURCE	IDENTIFIER
PB-EF1α-MCS-IRES-Neo	SBI	Cat# PB533A-2
PB-EF1α-MS2P_P65_HSF1	This Paper	N/A
PB-EF1α-MS2-LincGET	This Paper	N/A
PB-EF1α-MS2-LincGET(Δ1-650)	This Paper	Mutant from PB-EF1α-MS2-LincGET
PB-EF1α-MS2-LincGET(Δ651-1300)	This Paper	Mutant from PB-EF1α-MS2-LincGET
PB-EF1α-MS2-LincGET(Δ1301-1950)	This Paper	Mutant from PB-EF1α-MS2-LincGET
PB-EF1α-MS2-LincGET(Δ1954-2570)	This Paper	Mutant from PB-EF1α-MS2-LincGET
PB-EF1α-MS2-LincGET(Δ2761-3350)	This Paper	Mutant from PB-EF1α-MS2-LincGET
PB-EF1α-MS2-LincGET(Δ3351-3940)	This Paper	Mutant from PB-EF1α-MS2-LincGET
PB-EF1α-MS2-LincGET(Δ3941-4530)	This Paper	Mutant from PB-EF1α-MS2-LincGET
PB-EF1α-MS2-LincGET(Δ4531-5120)	This Paper	Mutant from PB-EF1α-MS2-LincGET
PB-EF1α-MS2-LincGET(Δ5121-5710)	This Paper	Mutant from PB-EF1α-MS2-LincGET
PB-EF1α-MS2-LincGET(Δ5710-6285)	This Paper	Mutant from PB-EF1α-MS2-LincGET
Software and Algorithms		
IMARIS	Bitplane	http://www.bitplane.com/
Photoshop CS6	Adobe	https://www.adobe.com/cn/products/photoshop.html
ImageJ	ImageJ	https://imagej.nih.gov/ij/
Bowtie2	Langmead and Salzberg, 2012	http://bowtie-bio.sourceforge.net/bowtie2/index.shtml
MACS2	Zhang et al., 2008	https://github.com/taoliu/MACS/

CONTACT FOR REAGENT AND RESOURCE SHARING

Further information and requests for resources and reagents should be directed to and will be fulfilled by the Lead Contact, Qi Zhou (qzhou@ioz.ac.cn).

EXPERIMENTAL MODEL AND SUBJECT DETAILS

Mouse embryos collection

All experiments were performed in accordance with ARRIVE (Animal Research: Reporting of *In Vivo* Experiments) guidelines and regulations. All of the animal experiments were performed under the ethical guidelines of the Institute of Zoology, Chinese Academy of Sciences. Procedures using animals were approved by the Institutional Animal Care and Use Committee of Institute of Zoology, Chinese Academy of Sciences. Two-cell stage embryos were collected from 6-week-old super-ovulated female ICR mice crossed with ICR males, 46 hours after the injection of human chorionic gonadotropin (hCG). One blastomere was injected with RNAs shown in Figure 2A at random.

Culture Cells

Mouse ESCs were cultured on a feeder layer in N2B27 medium supplemented with 2i (1 μM PD0325901 and 3 μM CHIR99021) and 20 ng/mL leukemia inhibitory factor (LIF). The mouse epiblast stem cells (mEpiSCs) was cultured in fibronectin coated dish in N2B27 medium plus 12 ng/mL bFGF (R&D, 233-FB-001MG/CF) and 10 ng/mL Activin A (R&D, 338-AC-01M) as described previously (Shuai et al., 2015). The culture medium was changed every day, and the mEpiSCs was digested to single cells by 0.05% trypsin/EDTA (GIBCO, 25300062) and passaged every 2 to 3 days. For cell transfection, the mEpiSCs line was passaged and seeded at a density of 1-1.5 × 10^4 cells/cm^2, after 2 days (60%–70% confluency), plasmid DNA (MS2-LincGET and MS2P-P65-HSF1) was transfected into cells using Lipofectamine 3000 transfection reagent (GIBCO, L3000015) according to the manufacturer's instructions. After transfection for 36 hours, cells were collected for further analysis.

METHOD DETAILS

RT-qPCR and 1C-qPCR

RNA was extracted using the RNeasy Mini Kit (QIAGEN, 74104) and the RNase-Free DNase Set (QIAGEN, 79254) was used to ensure that there was no DNA contamination. Reverse transcription was performed using a High Capacity cDNA Reverse Transcription Kit (ABI, 4368814). SYBR-qPCR was performed using a Power SYBR® Green PCR Master Mix (ABI, 4367659). TM-qPCR was

performed using a TaqMan Universal Master Mix II (Life, 4440048). 1C-qPCR was performed using a Single Cell-to-CT qRT-PCR Kit (Invitrogen, 4458237). All of these kits were used in accordance with the manufacturer's guidelines.

Plasmid vectors construction

In order to create Alexa Fluor 488-labeled RNA probes, the specific *LincGET* region (2,574-2,763), the specific *Dyei* region (384 – 642), and part of the *Egfp* sequence (362-668) as a control, were amplified using LongAmpTM *Taq* DNA Polymerase (NEB, M0534L). These sequences were sub-cloned into the plasmid pEASY-T3 cloning vector (TransGen, CT301-02), which contains the T7 promoter. For co-IP experiments involving the MS2 coat protein (MS2P), MS2-labeled *LincGET* and HA-labeled MS2P were cloned into the PB533A vector (SBI, PB533A-2) digested with *EcoR*I or SalI, respectively. *Carm1* (NM_021531 & NM_153141) overexpression vectors with CMV and T7 promoters and FLAG tag were bought from YouBio (YouBio, G156971 & G156972) and mixed equally. GFP-KASH sequence with T7 promoter for *in vitro* transcription was synthesized by BGI company and subcloned into pUC57 vector. *LincGET* and *Carm1* mutants were generated by PCR, 5′-phosphorylation, and ligation.

CARM1 fractionation

Four-cell stage embryos (about 500 embryos for each experiment) were lysed in 50 μL of lysis buffer (10 mM Tris-HCl (pH 7.4), 10 mM NaCl, 3 mM MgCl2 and 0.15% NP-40) for 10 min on ice. Immediately after lysis, samples were then centrifuge at 300 g at 4°C for 5 min. The supernatant was the cytoplasmic fraction and the precipitate was the nuclear fraction.

Micro-injection

We isolated 2-cell embryos from superovulated ICR female mice mated with normal males at 36 hours post-human chorionic gonadotropin (hCG) injection, and microinjected about 1-2 pL RNA at 150 ng/μL concentration into the nucleus of one blastomere of the 2-cell embryos, using an Eppendorf micromanipulator on a Nikon inverted microscope. The RNAs were *in vitro* transcribed with the mMESSAGE mMACHINE® T7 ULTRA Kit (Ambion, AMB1345-5), and the DNA templates with T7 promoter were amplified using LongAmpTM *Taq* DNA Polymerase (NEB, M0534L). Primers are shown in Table S5. PCR templates were plasmids shown in the KEY RESOURCES TABLE, except that for pancII17d where the template was the mouse genome DNA. When LNA was used in co-injection, 10 μM LNA for *Carm1* and 10 or 1 μM LNA for *LincGET* were used.

RNA pull-down

LincGET was *in vitro* transcribed with the mMESSAGE mMACHINE T7 ULTRA Kit (Ambion, AMB1345-5) and biotinylated with the Pierce RNA 3′ End Desthiobiotinylation Kit (Pierce, 20163) in accordance with the manufacturer's guidelines. A slot blot was then performed to demonstrate that RNAs had been efficiently biotinylated. Fifty picomoles of biotinylated RNA was heated to 85°C for 2 min, placed immediately on ice for at least 2 min and an equal volume of RNA structure buffer (10 mM Tris pH 7.0, 0.1 M KCl, 10 mM $MgCl_2$) was added. The samples were then moved to room temperature (RT) for at least 20 min to allow appropriate secondary structure formation. Mouse embryonic stem cells (mESCs), or early 4-cell stage embryos (approximately 2,600 embryos were used for each experiment) were digested with the Pierce IP Lysis Buffer (Pierce, 87787), supplied with Protease Inhibitor Cocktail (Pierce, 78441), and used in accordance with the manufacturer's protocols. RNA-pull down was then performed using the Pierce Magnetic RNA-Protein Pull-Down Kit (Pierce, 20164) according to the manufacturer's protocol. The retrieved protein was then detected by western blotting or Mass spectrometry.

Western blotting

The protein retrieved by RNA pull-down assay, or from 200 single blastomeres from 2-cell stage embryos digested with Pierce IP Lysis Buffer (10 μL/lane), were mixed with 30 μL of sample buffer (10 mL; 1.25 mL 0.5 M-pH 6.8-Tris-HCl, 2.5 mL glycerin, 2 mL 10% SDS, 200 μL 0.5% bromophenol blue, 3.55 mL H_2O and 0.5 mL β-mercaptoethanol) and incubated for 5 min in boiling water. The samples were then separated by SDS-PAGE with a 5% stacking gel (10 mL; 5.7 mL ddH_2O, 2.5 mL 1.5M pH 6.8 Tris-HCl, 1.7 mL 30% acrylamide (acryl:bis acryl = 29:1), 100 μL of 10% SDS, 50 μL of 10% ammonium persulfate and 10 μL of TEMED) and a 10% separating gel (10 mL; 4.1 mL ddH_2O, 2.5 mL 1.5M pH 8.8 Tris-HCl, 3.3 mL 30% acrylamide (acryl:bis acryl = 29:1), 100 μL of 10% SDS, 50 μL of 10% ammonium persulfate and 5 μL of TEMED) at 100 V for 1 hour. Separated proteins were then electrophoretically transferred onto a nitrocellulose membrane at 200 mA for 1 hour at 4°C. Membranes were then blocked in TBST buffer (10 mM Tris, 150 mM NaCl, 0.1% Tween 20, pH 7.4) containing 3% BSA (Sigma, B2064), for 1 hour at RT and then incubated with primary antibody, diluted in TBST containing 1% BSA, overnight at 4°C. After three washes for 10 min each in TBST, membranes were incubated for 1 hour at RT with the fluorescence secondary antibody diluted in TBST. After three washes for 10 min each, the fluorescence signals were quantified using Odyssey software.

Mass spectrometry

Mass spectrometry analysis was performed by BGI Company. Bound proteins were resolved by SDS-PAGE. The section of SDS-PAGE gel containing the protein sample was cut from gels, washed twice with 25 mM NH_4HCO_3 and 50% acetonitrile (1 hour each time), and dehydrated by the addition of 500 μL acetonitrile. Disulfide bonds were cleaved for spots by incubating the samples for 60 min at 56°C with 200 μL of 10 mM DTT in 25 mM NH_4HCO_3 buffer, and alkylation of cysteines was performed by the addition of

200 μL of 55 mM iodoacetamide in 25 mM NH_4HCO_3 buffer and incubating the samples for 45 min at room temperature in darkness. The spots were then dehydrated again with 500 μL acetonitrile after washing twice with 25 mM NH_4HCO_3. Trypsin (Promega) solution (10 ng/μL in 25 mM NH_4HCO_3 buffer) was then added for 37°C overnight digestion which was stopped by the addition of 5% formic acid. Finally, the extracts were dried under the protection of N_2. Samples were reconstituted in 3 μL of 0.1% trifluoroacetic acid (TFA) prior to MS analysis.

LC-ESI-MS/MS analyses were based on Orbitrap. After protein digestion, each peptide sample was desalted using a Strata X column (Phenomenex), vacuum-dried and then resuspended in a 200 μL volume of buffer A (2% Acetonitrile, 0.1% Formic acid). After centrifugation at 20,000 g for 10 min, the supernatant was recovered to obtain a peptide solution with a final concentration of approximately 0.5 μg/μl. Ten-microlitres of supernatant were loaded on a LC-20AD nanoHPLC (Shimadzu, Kyoto, Japan) by the autosampler onto a 2 cm C18 trap column. The peptides were then eluted onto a 10 cm analytical C18 column (inner diameter 75 μm) packed in-house. The samples were loaded at 8 μL/min for 4 min, then the 44 min gradient was run at 300 nL/min starting from 2 to 35% B (98% Acetonitrile, 0.1% Formic acid), followed by a 2-min linear gradient to 80%, and maintenance at 80% B for 4 min, finally returning to 5% in 1 min.

The peptides were subjected to nanoelectrospray ionization followed by tandem mass spectrometry (MS/MS) in a LTQ Orbitrap Velos (Thermo) coupled online to the HPLC. Intact peptides were detected in the Orbitrap at a resolution of 60,000. Peptides were selected for MS/MS using collision induced dissociation (CID) operating mode with a normalized collision energy setting of 35%. Ion fragments were detected in the LTQ. A data-dependent procedure that alternated between one MS scan followed by 10 MS/MS scans was applied for the 10 most abundant precursor ions above a threshold ion count of 5,000 in the MS survey scan with the following Dynamic Exclusion settings: repeat counts, 2; repeat duration, 30 s; and exclusion duration, 120 s. The applied electrospray voltage was 1.5 kV. Automatic gain control (AGC) was used to prevent overfilling of the ion trap; 1×10^4 ions were accumulated in the ion trap to generate CID spectra. For MS scans, the m/z scan range was 350 to 2,000 Da.

Immunoprecipitation

Magnetic Beads Protein G were coated with 5 μg of primary antibody in RIP wash buffer (50 mM Tris–HCl, pH 7.4, 150 mM sodium chloride, 1 mM $MgCl_2$, and 0.05% NP-40) containing 5% BSA overnight with rotation at 4°C. Then, we collected approximately 1×10^6 mESCs expressing HA-MS2P, with or without MS2-*LincGET,* and added 100 μL of RIP lysis buffer (150 mM NaCl, 50 mM Tris-HCl pH 7.4, 1 mM EDTA, 0.1% SDS, 1% NP-40, 0.5% sodium deoxycholate, 0.5 mM DTT, 1 mM PMSF/cocktail) and 10 μL of RNase inhibitor (Ambion, AM2694) followed by incubation on ice for 10 min. Next, we centrifuged the RIP lysate at 14,000 rpm for 10 min at 4°C, removed 100 μL of the supernatant and added this to 900 μL of beads-antibody complex in RIP Immunoprecipitation Buffer (860 μL RIP wash buffer, 35 μL 0.5 M EDTA, and 5 μL RNase inhibitor), and incubated this with rotation overnight at 4°C. The residual 10 μL of the supernatant of RIP lysate was treated as input. After washing, the immunoprecipitate were divided into two, one part was mixed with 15 μL of western blotting sample buffer and incubated for 5 min in boiling water; this blot was used to detect CARM1 and HA-MS2P. The other part was treated with proteinase K at 55°C for 30 min with shaking to digest the protein, followed by RNA extraction from the supernatant; RT-PCR was then performed to detect *LincGET*.

Northern blotting

Total RNAs in 500 embryos of each stage from 1- to 8-cell were extracted using the RNeasy Mini Kit (QIAGEN, 74104) and the RNase-Free DNase Set (QIAGEN, 79254) was used to ensure that there was no DNA contamination. Total RNAs were run on 15% urea-PAGE gels (15 mL; 7.2 g Urea, 1.5 mL 10 × TBE, 5.6 mL 40% acrylamide (acryl:bis acryl = 19:1), 75 μL 10% ammonium persulfate, and 15 μL TEMED) at 45 mA for 1 hour. The gels were then soaked for 5 min in a 0.5–1 μg/mL solution of ethidium bromide in 1 × TBE, and visualized using a UV transilluminator. After staining, RNAs were transferred to a nylon membrane (Life) by electroblotting at 200 mA for at least 1 hour. After blotting, the RNAs were crosslinked to the membranes using a commercial UV-crosslinking device (120 mJ burst over 30 s). We then pre-hybridized the membrane in 10 mL pre-hybridization solution (6 × SSC (Sigma), 10 × Denhardt's solution (Invitrogen), 0.2% SDS) for at least 1 hour at 65°C. Next, we hybridized the membrane in 10 mL hybridization solution (6 × SSC, 5 × Denhardt's solution, 0.2% SDS) containing 0.1 μM 3′ end-DIG-labeled single strand DNA oligonucleotide (Table S5, BGI company) for 16 hours with gentle agitation at room temperature (RT). The membrane was then washed three times with 10 mL wash solution (6 × SSC, 0.2% SDS) with gentle agitation at RT for 5 min, and washed once at 42°C for 10 min. After the final wash, signals were detected using the DIG detection kit (Roche, #11093657910) according to the manufacturer's protocol.

Immunofluorescence staining

Mouse embryos were fixed in 4% PFA for 30 min at RT, followed by permeabilization in normal permeabilizing solution overnight at 4°C. Embryos were then blocked in blocking solution (1% BSA in 1 × PBS) for 1 hour at RT after 3 washes for 5 min each in washing solution (0.1% Tween-20, 0.01% Triton X-100 in 1 × PBS), followed by incubation with primary antibody diluted with blocking solution overnight at 4°C. After 3 washes for 5 min each in washing solution, embryos were incubated with Alexa series fluorescent tag-conjugated secondary antibody diluted with washing solution for 1 hour at RT. After 3 washes in washing solution, nuclei were stained with DAPI (10 μg/mL in 1 × PBS) for 7 min. Imaging of Embryos in microdroplet in a dish were then performed directly after 3 washes, using laser-scanning inverted confocal microscope (LSM 780).

RNA-FISH and IF combining RNA-FISH

RNA-FISH and IF-coFISH were performed as described previously (Namekawa and Lee, 2011) except that probes were labeled by *in vitro* transcription using the MEGAshortscript Kit (Ambion, AM1354) with ATP, CTP, GTP, and ChromaTide Alexa Fluor 488-5-UTP (Invitrogen, C11403) solution in which 80% of uracil was labeled by Alexa Fluor 488. After removal of the zona pellucida with acidic Tyrode's Solution (Sigma, T1788), mouse embryos were incubated in 1 × PBS containing 6 mg/mL BSA for 3 min. Then, embryos were transferred onto Superfrost/Plus microscope slides and dried as quickly as possible. Embryos were fixed and permeabilized in 1% paraformaldehyde (PFA) with 0.04% NP-40 on ice for 5 min followed by fixation in 1% PFA on ice for 5 min. Then, the slides were transferred into 70% ethanol on ice. Slides were kept in 70% ethanol on ice until dehydration for RNA-FISH.

To perform immunofluorescence, slides were rinsed in PBS for 5 min, blocked in blocking buffer (PBS with 1% BSA, 0.1% Tween-20, and 0.4 U/μL of ribonuclease Inhibitor (Invitrogen, 10777019)) for 20 min at room temperature (RT), and incubated with primary antibody in blocking buffer for 1 hour at RT. After 3 washes with 0.1% Tween-20 in PBS, slides were incubated with secondary antibody in blocking buffer for 1 hour at RT. After 3 washes with 0.1% Tween-20 in PBS, slides were post-fixed in 4% PFA at RT for 10 min. Then, slides were transferred into 70% ethanol on ice after incubation in PBS for 5 min. Dehydration was performed in 80%, 95% and 100% Ethanol (× 2), with each incubation lasting for 5 min at RT. Slides were then dried for 5 min. Embryos were then hybridized in hybridization solution (50% Formamide (Sigma, F9037), 2 × SSC, 10% Dextran Sulfate (Sigma, 30915), 10 mM VRC (Sigma, 94742), 2 mg/mL BSA) containing 5 μg of Alexa Fluor 488-labeled RNA probes per slide at 37°C overnight (14-15 hours). After 3 washes for 5 min each in hybridization washing solution (50% Formamide, 2 × SSC) at 42°C and 4 washes for 5 min each in 2 × SSC, embryos were mounted with DAPI-Vectashield solution (Vector laboratories, H1200).

Microscopic analysis and three-dimensional reconstructions

Bright field images were acquired from embryos under a Nikon inverted Eclipse TS100 microscope equipped with a Digital Sight camera system (Nikon). Fluorescence staining was imaged using an inverted microscope (Leica, DMI3000B), laser-scanning inverted confocal microscope (LSM 780), or laser-scanning confocal microscope (Leica, TCS SP8). For three-dimensional (3D) reconstructions, blastocysts were fixed and stained with Phalloidin-Texas red (Invitrogen, T7471) to visualize the cell membrane, and confocal z stacks were taken at 1 μm intervals through the entire embryo. IMARIS software (Bitplane) was then used to outline cell membranes and then create 3D models of all cells within the embryo. Cells were then scored according to their relative position; cells completely surrounded by others were denoted as inner cells while those that had an outer surface were denoted as outer cells.

In vivo DNase I TUNEL assay

In vivo DNase I TUNEL assays were performed as described previously (Jachowicz et al., 2017). Embryos were injected at the 2-cell stage, collected at the 8-cell stage and washed twice with PBS. *In vivo* permeabilization was performed with 0.5% Triton X-100 in extraction buffer (50 mM NaCl, 3 mM $MgCl_2$, 0.5% Triton X-100 and 300 mM sucrose in 25 mM HEPES, pH 7.4) for 5 min on ice. Next, embryos were washed twice in extraction buffer without Triton X-100 and incubated with 1 U/μL of DNase I (Ambion, AM2222) in the same buffer for 5 min at 37°C. After fixation, TUNEL assays were performed with a Click-iT TUNEL Alexa Fluor Imaging Assay Kit (Life Technologies, C10247) according to the manufacturer's instructions. Finally, IF was performed as described earlier.

ATAC-seq library preparation and bioinformatic analyses of expression and heterogeneity in early embryo

Cells from ATAC-seq libraries created from approximately fifty 8-cell embryos were prepared as described previously (Wu et al., 2016). Briefly, samples were lysed in 5 μL of lysis buffer (10 mM Tris-HCl (pH 7.4), 10 mM NaCl, 3 mM $MgCl_2$ and 0.15% NP-40) for 10 min on ice. Immediately after lysis, samples were then incubated with the Tn5 transposase and tagmentation buffer at 37°C for 30 min (Vazyme Biotech, TD502). Then, the stop buffer was added directly into the reaction to end the tagmentation. PCR was then performed to amplify the library for 15 cycles using the following PCR conditions: 72°C for 3 min; 98°C for 30 s. This was by thermocycling at 98°C for 15 s, 60°C for 30 s and 72°C for 3 min, followed by 5 min at 72°C. After the PCR reaction, libraries were purified with 1.2 × AMPure (Backman, A63880) beads before proceeding to mitochondrial DNA depletion. A total of 400 sgRNAs targeting the mouse mitochondrial genome were provided as a gift by Wei Xie's laboratory of School of Life Sciences, Tsinghua University. Next, *in vitro* transcription was performed to produce sgRNAs using the MEGAshortscript Kit (Ambion, AM1354)). Each ATAC-seq library was incubated with 5 μg of sgRNA and 10 μg of Cas9 protein (PNA Bio, CP02-50) for 2 h at 37°C. After incubation, the reaction was treated by RNase A before being terminated by adding stop buffer (30% glycerol, 1.2% SDS, 250mM EDTA, pH 8.0).

The samples were then processed by an Illumina HiSeq 2500 sequencer with 50 bp paired-end sequencing reactions. Clean reads were then mapped to the mouse mm9 genome assembly by Bowtie2 (Langmead and Salzberg, 2012) using default settings. After this, reads with multiple genomic loci were discarded. Then, non-redundant reads were analyzed using MACS2 software (Zhang et al., 2008) to identify peaks (transcription factor binding sites) with a threshold of a p value less than 1×10^{-5}. Distributions of ATAC-seq read density around the transcription start sites (TSSs) regions (the upstream and downstream 1 kb regions, respectively) were plotted using Sitepro from the CEAS package (Shin et al., 2009) with a bin size of 20 bp. Finally, the ICM and TE

specific genes were reanalyzed from the published single cell RNA-Seq data in the GEO database GEO: GSE70605 (Liu et al., 2016).

To examine the transcript level of *LincGET* during mouse early embryo development, unique sequence from *LincGET* were identified by masking repeat elements, using cross_match engine in Repeat Masker (http://www.repeatmasker.org). The expression levels of *LincGET* during early embryo development (Figure S1B) was then calculated by Bowtie2 using published single-cell embryo RNA-seq datasets (GSE45719) (Deng et al., 2014). The levels of *Hprt transcript* were extracted from the same dataset. The blastomere-to-blastomere heterogeneity level of *LincGET* and *Hprt* in early-, middle-, late- 2-cell embryos and in 4-cell embryos (Figure 1A) were analyzed based on their transcript level in each early blastomere using algorithm from previous publication (Shi et al., 2015).

QUANTIFICATION AND STATISTICAL ANALYSIS

Statistical analyses [mean ± standard error of the mean (SEM)] for differential gene expression were performed in R. Levels of significance (Figures 1C, 1D, 1G, 1H, 2E, 2H, 3C, 4C, 5B–5G, 6C, 6E, 7A, 7C–7G, S3A, S6A, S6B, and S7E–S7H) were calculated with two tailed Student's t test. The correlation coefficient (r) and p value in Figure 4B are determined by Pearson's correlation. Two-sample Kolmogorov-Smirnov tests were used for statistical analysis in Figure 6D. Isoform abundance on SDS-PAGE gels (Figure 4C) was measured in ImageJ. For nuclear fluorescence intensity analysis (Figures 1D, 1H, 4A, 5B, 5C, 5F, 5G, 6C, 7C, 7D, S4, S6A, and S7F), nuclear regions for factor signal and DNA signal were separately cut out, discolored, inverted, and lined in one picture using Photoshop, then analyzed by ImageJ, and finally the ratio (× 100) of factor signal intensity to DNA signal intensity was used. For SOX2 fluorescence intensity analysis which localized in both cytoplasm and nucleus at 8-cell stage (Figure 5E), regions with same area for SOX2 signal and GFP signal were cut out, discolored, inverted, and lined in one picture using Photoshop, then analyzed by ImageJ, and finally the ratio (× 100) of SOX2 signal intensity to GFP signal intensity was used. In all figures: *, p value < 0.01; **, p value < 0.001 (Figures 5D and 6E); different letters between x and y (Figures 2E, 2H, 3C, and 7A), p value < 0.00001; different letters among a, b, c (Figures 7E–7G), p value < 0.01; NS (Figures 5D and S7E), p value > 0.05.

DATA AND SOFTWARE AVAILABILITY

Data Resources

The accession number for the ATAC-seq data reported in this paper is NCBI GEO: GSE110419. The original data of this paper has been uploaded onto Mendeley with the link as https://doi.org/10.17632/vc5tv49rdf.1.

Supplemental Figures

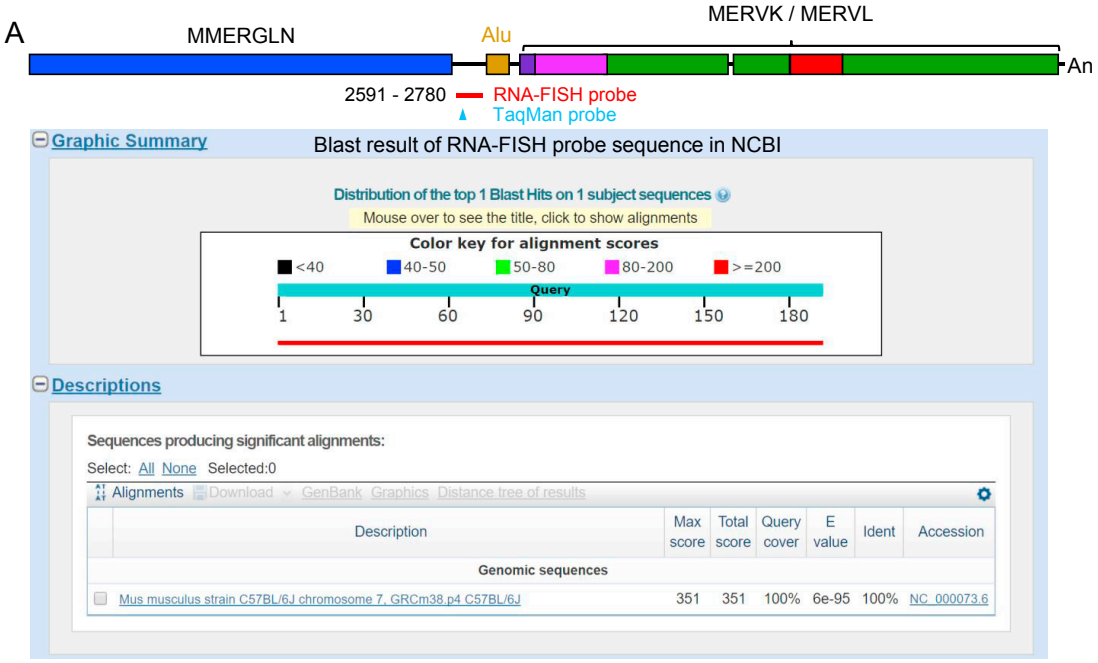

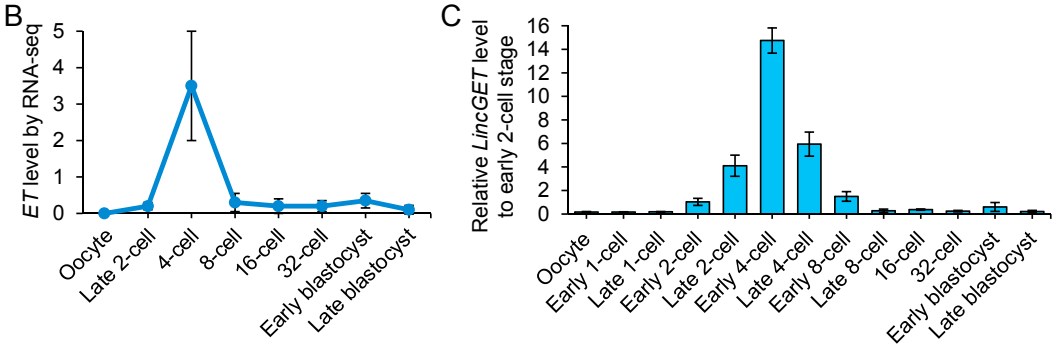

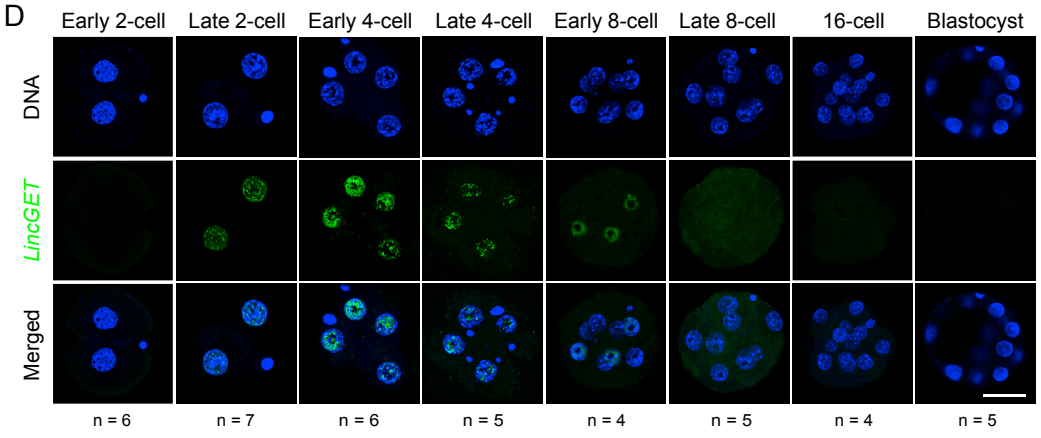

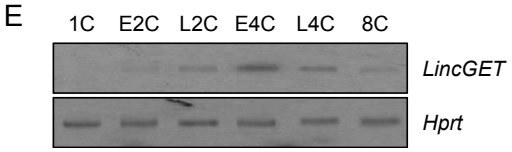

(legend on next page)

Figure S1. *LincGET* was Transiently Expressed and Asymmetrically Distributed in Two- to Four-Cell Blastomeres, Related to Figure 1

(A) NCBI blast result of *LincGET* probe sequence used in RNA-FISH. The result shows that the probe is specific for *LincGET*.

(B) Bioinformatic analysis showing transient *LincGET* expression at the 4-cell stage.

(C) Expression pattern of *LincGET* at different stages of preimplantation mouse embryos based on TM-qPCR. The error bars represent SEM. About 50 embryos of each stage were used and three experimental replicates were performed.

(D) RNA-FISH for *LincGET* in embryos at the early 2-cell to blastocyst stage, showing that *LincGET* is present in the nucleus of late 2- to 4-cell embryos, but weakly expressed in early 8-cell embryos. Three experimental replicates were performed. Scale bar, 50 μm.

(E) Northern blotting for *LincGET* in embryos at 1- to 8-cell stage. The results show that *LincGET* is expressed at late 2- to 4-cell embryos, but weakly expressed in early 8-cell embryos.

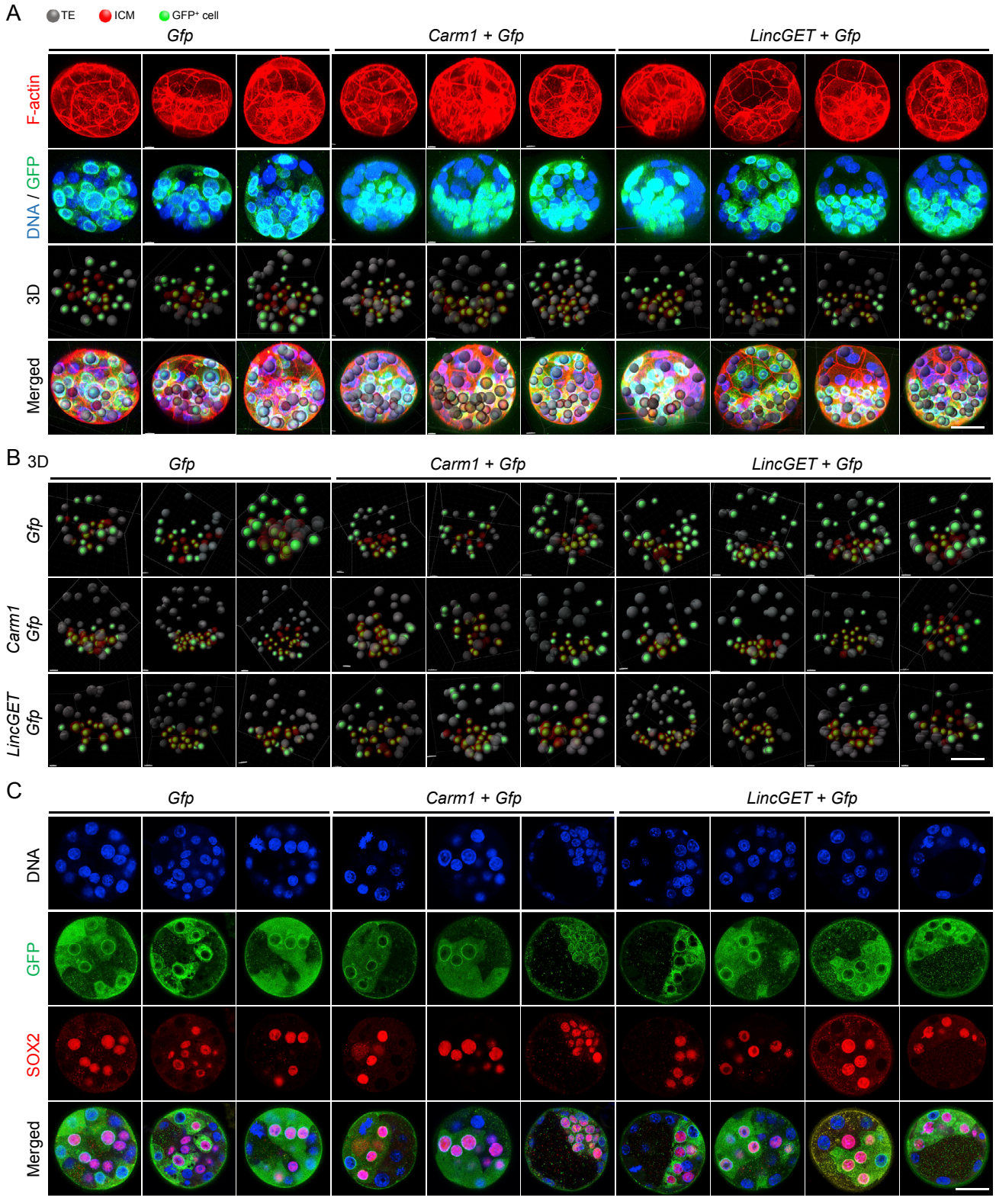

(legend on next page)

Figure S2. Increased *LincGET* Biased Blastomeres toward an ICM Fate, Related to Figure 2 and Tables S1, S2, and S3

(A and B) Examples of 3D analysis results. Scale bar, 50 μm.

(C) SOX2 and GFP fluorescent staining of blastocysts. SOX2 is used as the ICM marker. The results show that most SOX2-positive cells are GFP-positive in embryos injected with *Carm1* and *Gfp* (*Carm1* + *Gfp* lane) or *LincGET* and *Gfp* (*LincGET* + *Gfp* lane) but not those injected with only *Gfp* (*Gfp* lane). Three experimental replicates were performed. Scale bar, 50 μm.

A

Group	Blastocysts 3D (%)	Total cells (n)	Inner cells (%)	GFP cells (%)	Inner cells that are GFP+ (%)	GFP cells that are Inner (%)
Gfp	65 (82.65)	41.59 ± 8.79	37.68 ± 3.43	49.02 ± 3.44 [x]	53.06 ± 8.03 [x]	40.51 ± 4.60 [x]
Dyei	33 (82.50)	39.06 ± 6.41	37.12 ± 2.35	50.28 ± 2.11 [x]	54.26 ± 6.90 [x]	39.92 ± 4.10 [x]
pancII17d	38 (84.44)	38.79 ± 8.66	36.99 ± 3.09	48.38 ± 2.10 [x]	52.11 ± 5.95 [x]	39.64 ± 3.39 [x]
LincGET(1-2570)	34 (82.93)	39.44 ± 8.38	37.15 ± 3.16	49.47 ± 2.76 [x]	54.13 ± 5.49 [x]	40.48 ± 3.04 [x]
LincGET(3940-6285)	37 (86.05)	43.73 ± 11.53	36.94 ± 2.77	48.31 ± 1.91 [x]	51.38 ± 5.81 [x]	39.15 ± 3.90 [x]
antiAmp	35 (83.33)	40.57 ± 9.33	37.12 ± 3.05	50.25 ± 3.26 [x]	54.84 ± 6.92 [x]	40.31 ± 3.57 [x]

B

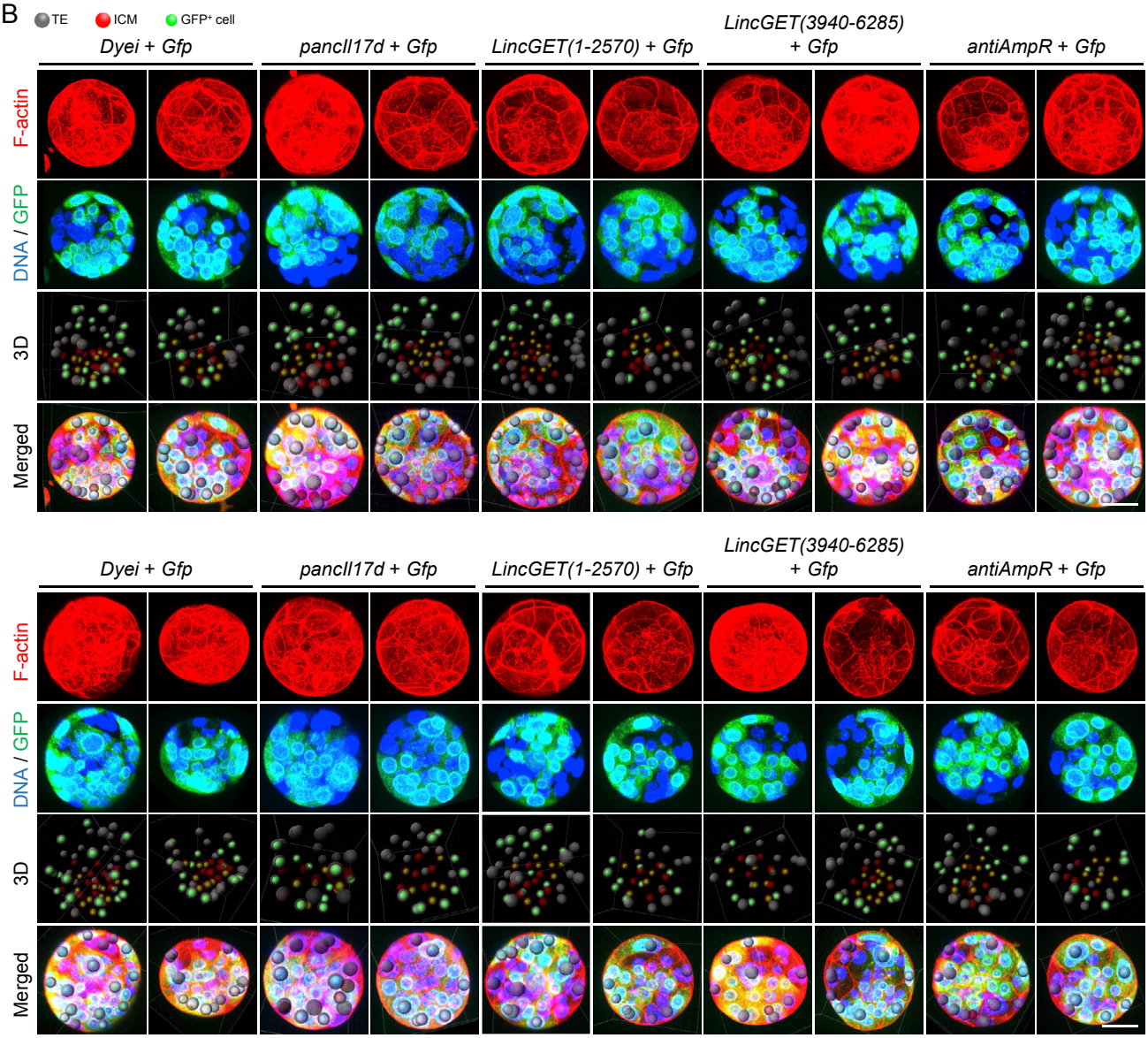

Figure S3. Overexpression of Control RNAs Cannot Bias Cell Fate of Injected Blastomeres, Related to Figure 2 and Table S2

(A) Analysis of the distribution of progeny of injected blastomeres at the blastocyst stage based on 3D reconstruction. Data are represented as mean ± SEM. Two-tailed Student's t tests were used for statistical analysis. Key to table headings: Blastocyst 3D (%) is the number and developmental rate of blastocysts that were

(legend continued on next page)

all used for 3D analysis; Total cells is the total number of cells in the blastocyst; Inner cells (%) is the percentage of inner cells out of the total number of cells in the blastocyst; GFP cells (%) is the percentage of GFP-positive cells out of the total number of cells in the blastocyst; GFP cells that are inner (%) is the percentage of GFP-positive inner cells out of the total number of GFP-positive cells in the blastocyst; Inner cells that are GFP^+ (%) is the percentage of GFP-positive inner cells out of the total number of inner cells in the blastocyst.
(B) Examples of 3D analysis results. Scale bar, 50 μm.

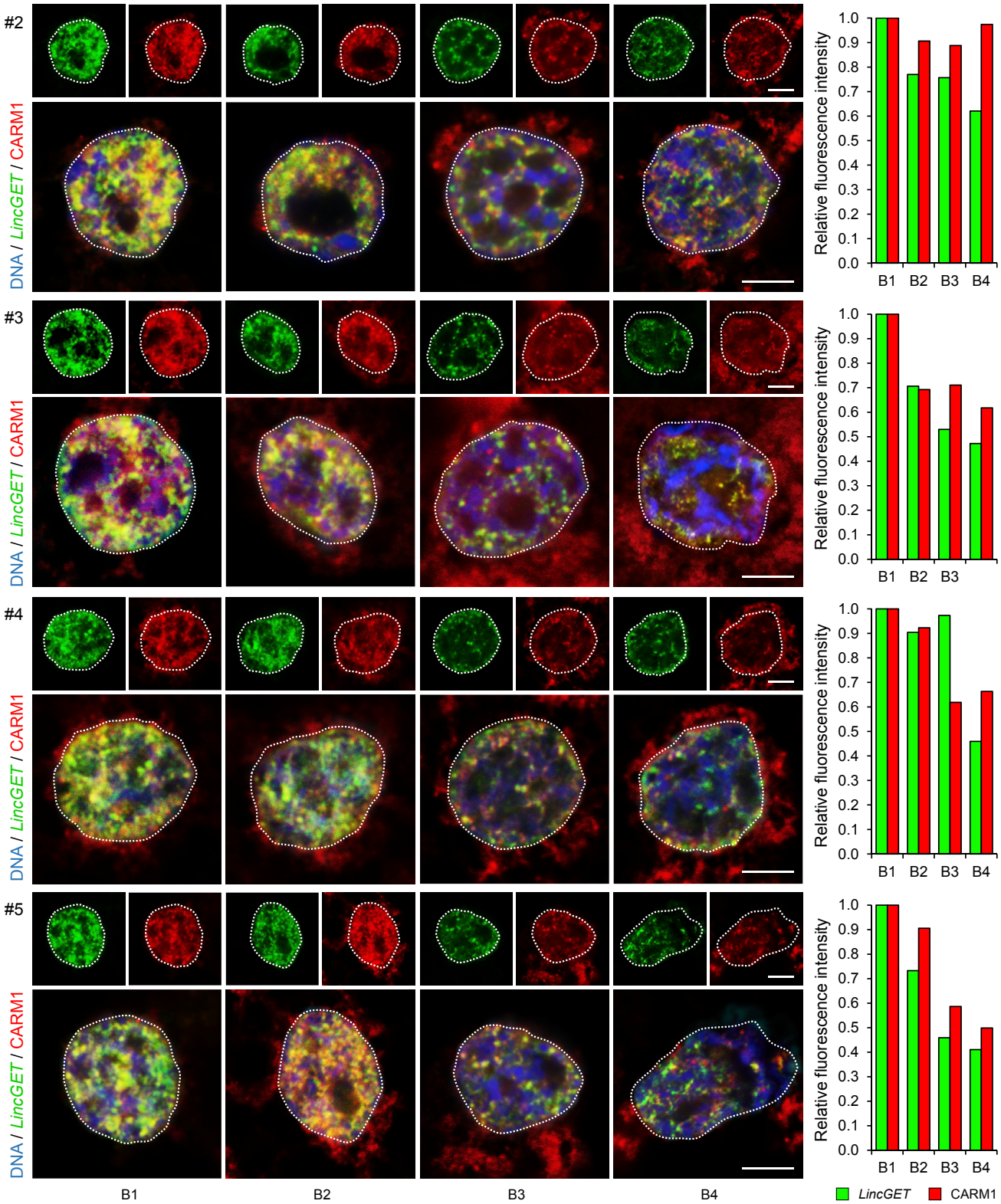

Figure S4. *LincGET* and CARM1 Co-localized in the Nucleus of Four-Cell Embryos with Linear Correlation, Related to Figure 4

IF combine with FISH results show co-localization of *LincGET* and CARM1 in the nucleus of 4-cell embryos with linear correlation. We used the relative intensity of *LincGET*/CARM1 (Green/Red) to nucleus DNA (Blue) as the final intensity for comparison, which could reduce errors caused by nucleus's depth between blastomeres. Scale bar, 10 μm.

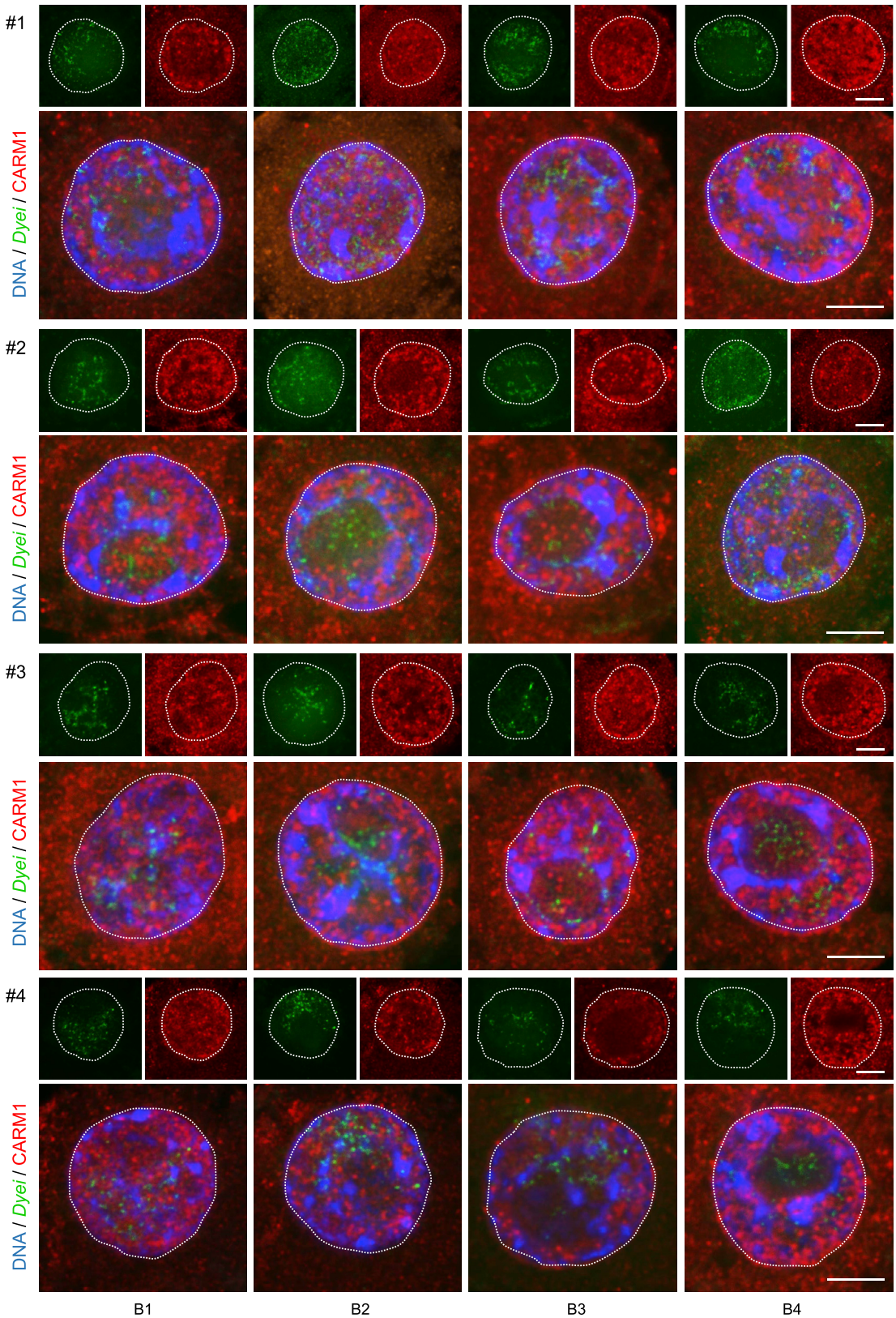

Figure S5. *Dyei* Do Not Co-localize with CARM1, Related to Figure 4

IF combine with FISH results show *Dyei* do not co-localize with CARM1. Scale bar, 10 μm.

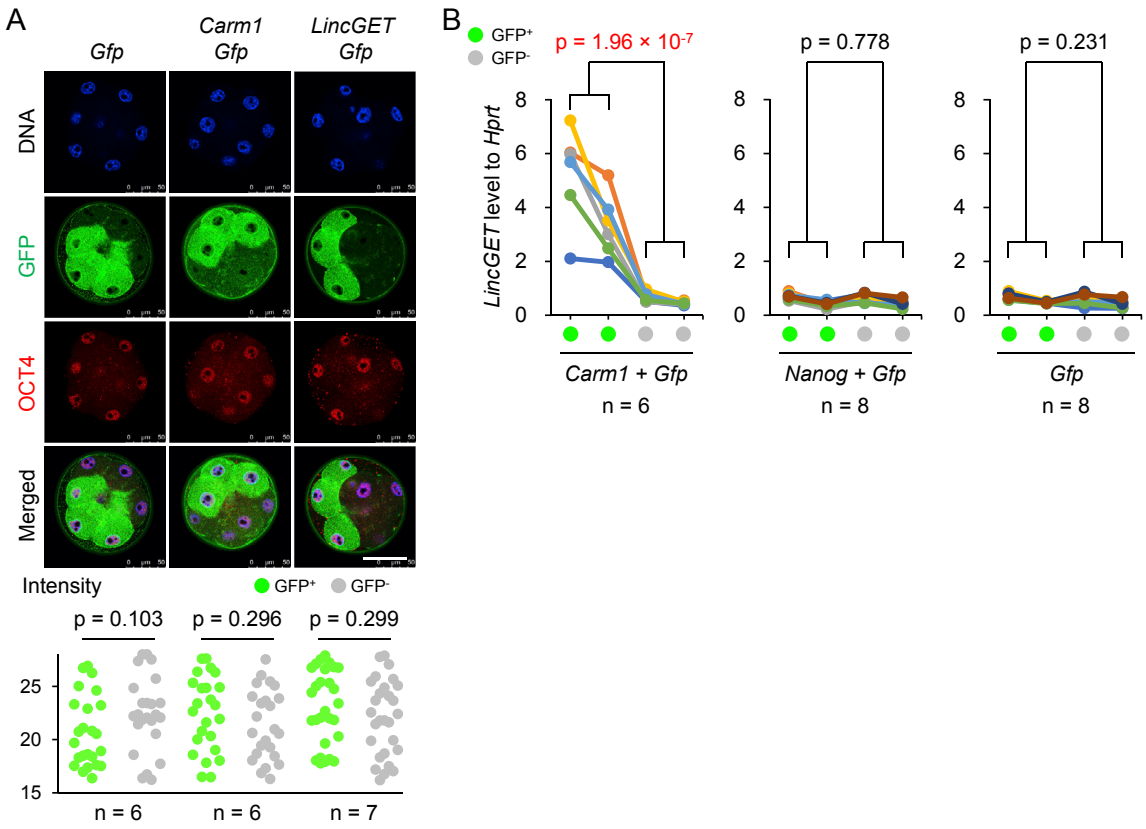

Figure S6. *LincGET*/CARM1 Complex Had No Effect on *Oct4* Expression, Related to Figure 5

(A) No change in OCT4 was found in the progeny of *Carm1*- or *LincGET*-injected blastomeres. Three experimental replicates were performed. Scale bar, 50 μm. For fluorescence analysis, the green ball stand GFP^+ cells and the gray ball stand for GFP^- cells. Two-tailed Student's t tests were used for statistical analysis.

(B) Single cell TM-qPCR analysis of *LincGET* expression level showing that overexpression of *Carm1* but not *Nanog* could activate *LincGET* at the 4-cell stage. Two-tailed Student's t tests were used for statistical analysis.

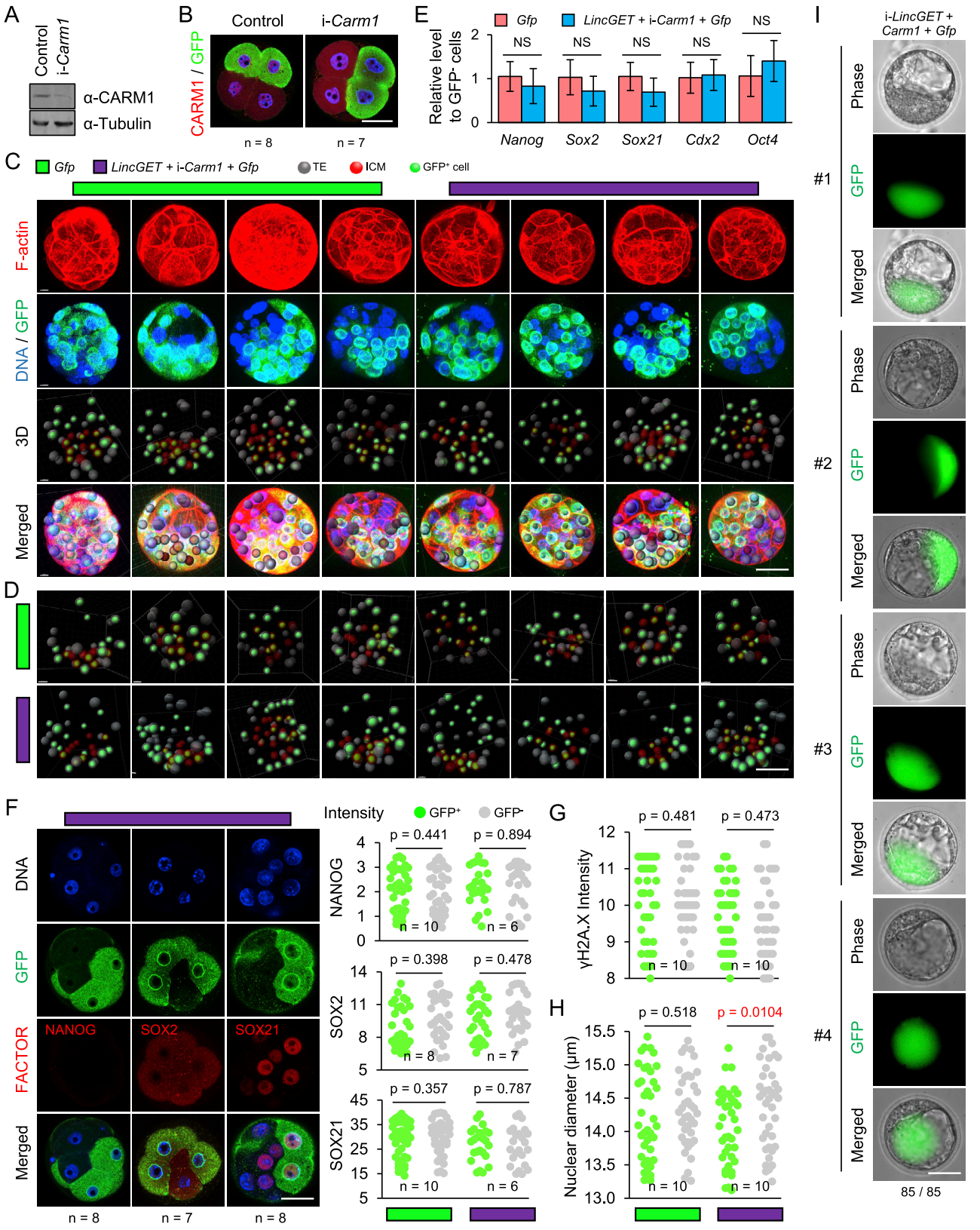

(legend on next page)

Figure S7. Interdependence between *LincGET* and CARM1 in Directing ICM Fate, Related to Figure 7

(A and B) Efficient ablation of *Carm1* using Locked Nucleic Acid (LNA) injection proven by western blot (A) and IF (B). Three experimental replicates were performed. i-, LNA interference. α-, anti-. Scale bar, 50 μm.

(C and D) Examples of 3D analysis results. The group names in (D) are same to that in (C). Scale bar, 50 μm.

(E) qPCR results show no change in *Nanog*, *Sox2*, *Sox21*, *Cdx2*, and *Oct4* in the progeny of blastomeres injected with *LincGET* and LNA (for *Carm1*). Three experimental replicates were performed. The error bars represent SEM. Two-tailed Student's t tests were used for statistical analysis. Compared to the *Gfp* group, NS, $p > 0.05$.

(F) Fluorescent staining of 8-cell embryos shows no change in NANOG, SOX2, and SOX21 in the progeny of blastomeres injected with *LincGET* and LNA (for *Carm1*). The group names are same to that in (C). For fluorescence analysis, the green ball represents GFP^+ cells and the gray ball represents GFP^- cells. Three experimental replicates were performed. Scale bar, 50 μm.

(G) Quantification of fluorescence intensity of γH2A.X shows no increased DNA damage in *LincGET*-overexpressing with *Carm1*-depleted blastomeres. The group names are same to that in (C). For fluorescence analysis, the green ball represents GFP^+ cells and the gray ball represents GFP^- cells. Three experimental replicates were performed. Two-tailed Student's t tests were used for statistical analysis.

(H) Quantification of nuclear volume of embryos in Figure 6F. The results show a slight decrease in nuclear volume in daughter cells of *LincGET*-overexpressing with *Carm1*-depleted blastomeres. The group names are same to that in (C). For fluorescence analysis, the green ball represents GFP^+ cells and the gray ball represents GFP^- cells. Three experimental replicates were performed. Two-tailed Student's t tests were used for statistical analysis.

(I) Depletion of *LincGET* led to late 2-cell stage arrest, and this could not be rescued by *Carm1* overexpression. Scale bar, 50 μm.